A New Vortex Flow Experiment for Computer Code Validation

D. Hummel
Institute of Fluid Mechanics, TU Braunschweig
Bienroder Weg 3, 38106 Braunschweig, Germany

G. Redeker
Institute of Design Aerodynamics, DLR Braunschweig
Lilienthalplatz 7, 38108 Braunschweig, Germany

Abstract

In this paper the present knowledge on the vortex formation on slender delta wings is summarized. The interference mechanisms between primary and secondary vortices as well as the vortex breakdown phenomenon are especially emphasized. The effects of Mach number and Reynolds number are treated separately and the differences in the flow around wings with sharp and rounded leading edges are discussed. The experimental details necessary for the validation of numerical methods are derived and a brief review of relevant modern experimental techniques is given. Finally a configuration suited for a new International Vortex Flow Experiment (VFE-2) as well as a corresponding test program are presented.

1 Introduction

At the beginning of the 1980's the status of the Euler methods for the calculation of vortical flows had reached such a high standard that good experimental data were necessary to validate the codes. This lead to the International Vortex Flow Experiment (VFE-1) [1] which has been carried out in 1984 – 1986: On a cropped delta wing with a leading-edge sweep of 65° combined with a fuselage, see Fig. 1, force and pressure distribution measurements as well as flowfield studies have been carried out for a certain variety of flow conditions in various wind tunnels worldwide. The results have been summarized in [2], and later the state of the art has been reviewed in [3], [4], [5].
Even for sharp leading edges with fixed primary separation the Euler codes are not well suited to calculate the pressure distribution on a slender wing properly, see Fig. 2, since the secondary separation is not modelled. In the last ten years considerable progress has been achieved in the numerical calculation of vortical flows by taking into account viscous effects through solutions of the Navier-Stokes equations [6], [7], [8]. This means that Reynolds number effects are now included and secondary vortices turn out. Laminar solutions tend to have convergence problems due to weak viscous damping. For turbulent flows in solutions of the Reynolds-averaged Navier-Stokes equations a turbulence model has to be applied which provides additional viscous damping in the boundary layers as well as in the viscous regions of the primary and secondary vortices. The pressure distribution on the upper surface of the wing is very sensitive to correct modelling of the viscous regions of the flowfield as shown in Fig. 2. If the grid resolution is fine enough reasonable pressure distributions turn out by taking into account the viscous effects, but different turbulence models lead to differences in

Paper presented at the RTO AVT Symposium on "Advanced Flow Management: Part A – Vortex Flows and High Angle of Attack for Military Vehicles", held in Loen, Norway, 7-11 May 2001, and published in RTO-MP-069(I).

Report Documentation Page

Form Approved
OMB No. 0704-0188

1. REPORT DATE	2. REPORT TYPE	3. DATES COVERED
00 MAR 2003	**N/A**	**-**

4. TITLE AND SUBTITLE	5a. CONTRACT NUMBER
A New Vortex flow Experiment for Computer Code Validation	5b. GRANT NUMBER
	5c. PROGRAM ELEMENT NUMBER
6. AUTHOR(S)	5d. PROJECT NUMBER
	5e. TASK NUMBER
	5f. WORK UNIT NUMBER
7. PERFORMING ORGANIZATION NAME(S) AND ADDRESS(ES) **NATO Research and Technology OrganisationBP 25, 7 Rue Ancelle, F-92201 Neuilly-Sue-Seine Cedex, France**	8. PERFORMING ORGANIZATION REPORT NUMBER
9. SPONSORING/MONITORING AGENCY NAME(S) AND ADDRESS(ES)	10. SPONSOR/MONITOR'S ACRONYM(S)
	11. SPONSOR/MONITOR'S REPORT NUMBER(S)

12. DISTRIBUTION/AVAILABILITY STATEMENT
Approved for public release, distribution unlimited

13. SUPPLEMENTARY NOTES
Also see: ADM001490, Presented at RTO Applied Vehicle Technology Panel (AVT) Symposium held inLeon, Norway on 7-11 May 2001, The original document contains color images.

14. ABSTRACT

15. SUBJECT TERMS

16. SECURITY CLASSIFICATION OF:			17. LIMITATION OF ABSTRACT	18. NUMBER OF PAGES	19a. NAME OF RESPONSIBLE PERSON
a. REPORT	b. ABSTRACT	c. THIS PAGE			
unclassified	**unclassified**	**unclassified**	**UU**	**32**	

Standard Form 298 (Rev. 8-98)
Prescribed by ANSI Std Z39-18

the pressure distributions. Looking into more details of these calculations according to Figs. 3 and 4, large differences concerning the total pressure distribution and the eddy viscosity contours are present: The Baldwin-Lomax turbulence model [9] (with the Degani-Schiff [10] modification) provides eddy viscosity only in the boundary layers, whereas the Wilcox k - ω turbulence model [11] shows eddy viscosity within the primary and the secondary vortex. Only the correct prediction of the secondary separation line and of the structure of the secondary vortex lead to the right lateral and vertical position of the primary vortex and hence to the correct suction peak in the pressure distribution. All calculations for viscous flows shown in Figs. 2 - 4 have been carried out for fully turbulent boundary layers and regions with laminar boundary layers have not been taken into account.
In the present paper the vortex formation on the upper surface of slender wings will be described in some detail and the interference mechanisms between the vortices as well as the vortex breakdown phenomenon are especially emphasized. The effects of Mach number and Reynolds number are treated separately for sharp and rounded leading edges. For the validation of numerical methods the required experimental details are derived and a review of relevant modern experimental techniques is given. Finally a configuration for a new International Vortex Flow Experiment (VFE-2) and a corresponding test program will be presented.

2 Notations

$A = b^2/S$	Aspect ratio
M	Free stream Mach number
$R = Vc/\nu$	Free stream Reynolds number
$R_{tr} = Vx_{tr}/\nu$	Transition Reynolds number
S	Wing area
V	Free stream velocity
b	Wing span
$c = c_R = c_i$	Wing root chord
$\bar{c}$	Mean aerodynamic chord
$c_p = (p - p_\infty)/q_\infty$	Pressure coefficient
p	Static pressure
p_t	Total pressure
$p_{tt} = 1 - (p_t/p_{t\infty})$	Total pressure loss
q_∞	Free stream dynamic pressure
r_{LE}	Streamwise leading-edge radius
t	Wing thickness
x, y, z	Wing apex-fixed coordinates
Λ	Leading-edge sweep
α, β	Angle of attack, sideslip
$\eta = 2y/b_{local} = y/s_1$	Dimensionless spanwise coordinate
μ_t (muet = μ_t/μ)	Dynamic eddy viscosity
ν	Kinematic viscosity

3 Description of the vortical flowfield

3.1 Wings with sharp leading edges

3.1.1 Basic vortex formation

On a sharp-edged slender delta wing inclined against the free stream at an angle of attack α, according to Fig. 5 the flow on the lower side moves outboard. Flow separation takes place at the sharp leading edge and a primary vortex is formed over the upper surface of the wing. Underneath this vortex an attached flow is established with an attachment line located at the centre-line or at some spanwise position between the centre-line and the leading edge, depending on the angle of attack. The flow near the wing surface is directed outboard and after having passed the suction peak underneath the primary vortex axis the steep adverse pressure gradient towards the leading edge causes flow separation. The separation line is clearly indicated in Fig. 5 and a secondary vortex is formed in the region close to the leading edge. Under certain circumstances even a tertiary separation can be observed underneath the secondary vortex [12], [16].
On both sides of the wing the boundary layer flow starts laminar at the apex and far more downstream transition to the turbulent state will take place depending on the Reynolds number. The turbulent boundary layer status can also be triggered by means of a turbulence generator as shown in Fig. 6 for the upper surface. In this case the secondary separation line is shifted towards the leading edge and compared with the laminar case (Fig. 5) a smaller secondary vortex is generated. Concerning the pressure distribution there exists a remarkable effect of the upper surface boundary layer status as shown in Fig. 7: The large secondary vortex resulting from the separation of a laminar boundary layer shifts the primary vortex upwards and inboard compared with the inviscid case represented in Fig. 7 by the slender body theory of J.H.B.Smith [13]. Therefore the suction peak is considerably reduced. On the other hand the strong secondary vortex itself induces large additional suction and this leads to a second suction peak in the pressure distribution of about the same amount. In the case of the separation of a turbulent boundary layer the smaller secondary vortex leads to a lower shift of the primary vortex. Correspondingly the suction peak is larger and due to the smaller additional suction induced by the secondary vortex a pressure distribution with a single suction peak turns out. Thus the shape of the pressure distribution is a clear indication for the status of the boundary layer at a certain station of the wing. In Fig. 8 the two types of pressure distributions are shown for a fully laminar case and for an artificially turbulent case. It is interesting to note that although the pressure distribution strongly depends on the status of the boundary layers the overall forces and moments are the same in the laminar and the turbulent case since the area underneath the pressure distribution remains virtually unchanged.

3.1.2 Effects of Reynolds number

For wings with sharp leading edges the flow separation is fixed to the leading edges and a Reynolds number effect on the primary separation does not exist. Nevertheless the boundary layer formation depends on the Reynolds number. For low Reynolds numbers the flow is laminar everywhere on the lower surface and between the secondary separation lines on the upper side, see Fig. 5. With increasing Reynolds number the flow becomes turbulent in the rear part of the wing, and this leads to an outboard shift of the secondary separation line on the upper side. For a given wing the Reynolds number $R_{tr} = Vx_{tr}/\nu$, based on the distance x_{tr} of the transition point from the wing apex, is only a function of the angle of attack α as

shown in [14] for an A = 1.0 delta wing. The comprehensive data set provided by NASA [15] for the sharp-edged 65° delta wing contains low speed measurements only for $R = 6 \bullet 10^6$ at which the upper surface boundary layer was already mainly turbulent. The same is true for M = 0.85 and according to Fig. 9 there are no Reynolds number effects up to $R = 36 \bullet 10^6$.

3.1.3 Effects of Mach number

Within the VFE-1 program the main investigations have been carried out at M = 0.85, but a certain variation of Mach number including incompressible flow has been considered. Later this configuration has been tested again by NASA [16] in the Mach number range $0.4 \leq M \leq 1.6$ at Reynolds numbers $2.5 \bullet 10^6 \leq R \leq 5.4 \bullet 10^6$. In some cases the boundary layers were laminar in the front part and turbulent in the rear part of the wing. With increasing Mach number the primary vortex moves inboard and its suction peak in the surface pressure distribution decreases. The flow becomes supercritical within the primary vortex and a crossflow shock is formed for $M \geq 0.6$ at an angle of attack $\alpha = 20°$, increasing in strength with increasing Mach number. At first the laminar boundary layer separation and later also the turbulent boundary layer separation become fixed to the crossflow shock location. For Mach numbers M > 0.8 a terminating normal shock occurs between the primary vortices in the rear part of the wing, and this shock reaches the trailing edge of the wing at $M \cong 0.95$. Quantitative details of the flowfield with crossflow and terminating shocks are not available. Fig. 10 shows an example from the comprehensive NASA data for the 65° delta wing [15]: All compressibitity effects discussed so far may be taken from the overall forces and moments as well as from the pressure distributions, but a detailed flow analysis has not been carried out.

3.1.4 Vortex breakdown

For large angles of attack vortex breakdown takes place within the primary vortices. On a delta wing with a leading-edge sweep of 65° this phenomenon occurs for angles of attack $\alpha \geq 20°$. Vortex breakdown has been described for the first time in [17] and since that time a huge number of investigations on this subject has been carried out worldwide, which will not be described in all details here. Out of the two possible modes of vortex breakdown discussed in [18] the spiral type occurs in the flowfield of slender delta wings. Today it is common understanding that the flow past a slender delta wing at large angles of attack becomes unsteady even for a fixed wing. This means in other words that for large angles of attack and steady boundary conditions only unsteady solutions of the Euler and the Navier-Stokes equations do exist. The spiral-type vortex breakdown is well predicted by numerical solutions of the Navier-Stokes equations [19], [20], [21], [22], [23], [24], see Fig. 11: The instantaneous vortex axis spirals in space against the sense of the primary vortex and this spiral turns around with respect to time in the sense of the primary vortex, and in the centre of the spiralling motion a region of reversed flow is present. Correspondingly all quantities of the flowfield, the pressure distribution on the wing as well as the overall forces and moments show oscillations. A detailed frequency analysis [22], [24] reveals three dominating frequencies: The most important one is related to the azimuthal mode described so far, but an axial and a radial mode, each with a corresponding frequency, do also exist. These three modes and frequencies are well confirmed by experimental data [25], [26] measured on different delta wings but unfortunately experimental data are not available for those configurations, which were subject to calculations.

The determination of the vortex breakdown position on the wing is a problem in experimental investigations as well as in numerical calculations. For comparisons the same definitions of the breakdown location should be used, e.g. starting point of the spiralling motion of the vortex axis or the onset of reversed flow. An attempt to correlate properly evaluated experimental data with numerical calculations for the experimental conditions is presently under way within the AVT Working Group 080 [27]. The vortex breakdown position is always located in a region with adverse pressure distribution in axial direction. Therefore it starts at a certain angle of attack in the vicinity of the trailing edge of the wing and moves upstream over the wing with increasing angle of attack. The vortex breakdown position is not very sensitive to Reynolds number and Mach number. In high subsonic and in supersonic flows the terminating shock causes a strong pressure increase in axial direction, and its relation to vortex breakdown is treated in [28].

3.1.5 Deadwater-type flow

With increasing angle of attack the vortex breakdown position within the primary vortices moves upstream over the wing, see Fig. 12, and at a certain angle of attack the wing apex is reached. According to [29], this happens for the VFE-1 configuration at an angle of attack of $\alpha = 43°$. The pressure distribution on the whole upper surface of the wing suddenly jumps to a constant value and the corresponding flow is a separated flow with deadwater-type structure. As shown in [22] and [24], for angles of attack $\alpha > 43°$ the pressure distribution and the overall forces and moments are well predicted by unsteady Euler and Navier-Stokes solutions.

3.2 Wings with rounded leading edges

Within the scope of the original vortex flow experiment on the VFE-1 configuration a rounded leading edge has been studied as well [1], [2]. The comprehensive data set provided by NASA [15] contains pressure distribution and balance measurements on the 65° delta wing with three different rounded leading edges at various Reynolds and Mach numbers. Finally in Germany the hypersonic configuration ELAC-1, which consists of a blunt body with elliptic cross sections, has been tested in a wide range of Reynolds and Mach numbers in various wind tunnels [30].

These investigations on wings with rounded leading edges show that the basic flow pattern described in section 3.1 for sharp edged wings occurs in the same way also for wings with rounded leading edges. Reynolds and Mach number effects on the suction side flow are virtually the same as for sharp-edged wings. The principal difference is the fact, that at rounded leading edges the primary separation is no longer fixed and new effects result from the dependence of the primary separation on curvature radius and Reynolds number. Fig. 13, taken from [15], indicates that on the wing with rounded leading edges at low angles of attack the flow remains attached at the rounded leading edges in the front part of the wing. High suction peaks are found in the vicinity of the leading edge and flow separation takes place only in the rear part of the wing where the leading edge radii are small. With increasing angle of attack the region of separated flow becomes larger. For low Reynolds numbers the primary separation takes place just at the leading edge, but for high Reynolds numbers the region of attached flow increases. The primary separation line moves to the upper surface of the wing and again strong suction peaks occur in the pressure distribution at the leading edge.

3.3 Unsteady vortical flows

A 65° delta wing has been investigated in rolling motion [31] and the VFE-1 configuration has also been tested in pitching, rolling and yawing motion. The complete results of these measurements at DLR Braunschweig are available in [32] and some data for the pitching motion at various angles of attack may be taken from [29]. A similar configuration with a modified thickness distribution has been tested recently by means of unsteady PSP measurements at DLR Göttingen [33]. Euler and Navier-Stokes codes have also been applied for the calculation of pitching [34], [35], [36] and rolling [37], [38], [39], [40] delta wings. The overall characteristics are well predicted by Navier-Stokes codes, but experimental details for comparison are missing.

4 Experimental needs

In calculations of the vortical flow around a delta wing by means of the Reynolds-averaged Navier-Stokes equations a turbulence model has to be used and the Figs. 2 to 4 show typical examples for the differences in the results for different turbulence models. For the validation of Navier-Stokes codes many experimental details of the flowfield are needed which are far beyond the scope of the measurements on the VFE-1 configuration. These needs are listed subsequently:

1) The location of the transition line on the upper and the lower surface of the wing should be determined in order to know the status of the boundary layers and to adapt numerical calculations to experimental conditions. Apart from this, a data base on this subject is also necessary for the validation of future methods for the prediction of the laminar/turbulent transition on slender delta wings.
2) More detailed surface pressure distributions are necessary to identify the effects of primary, secondary and tertiary separations. For this purpose reliable and accurate methods should be used which are not based on surface pressure taps, since wind tunnel models with pressure taps are very complicated and they provide only a limited number of sections which have to be fixed a priori.
3) There exists an urgent need of experimental data on the structure of the boundary layers on the wing. The only existing study of the 3D boundary layers on a delta wing has been published in [41] for laminar flow on upper and lower surface. Similar measurements for 3D turbulent boundary layers are missing. The distributions of total pressure, velocity and vorticity components, turbulent energy and eddy viscosity e.g. are necessary for comparisons with numerical results according to different turbulence models.
4) The distributions of magnitude and direction of the wall shear stress and the position of the separation lines on the surface of the wing are necessary from experiments for comparison with numerical results. For this purpose direct measurements of the shear stress have to be considered, since oilflow pictures from the surface cannot be carried out in modern facilities such as cryogenic wind tunnels.
5) The positions of the primary, secondary and tertiary vortices relative to the wing are needed for comparison with numerical results.
6) The structure of the viscous regions of the flowfield has to be analysed in detail experimentally in order to be able to judge whether the various CFD codes and turbulence models describe these details properly. Regions of special interest in this respect are the shear layer and the viscous core of the primary vortex as well as the secondary and the tertiary vortices.

7) The investigations according to 1) to 6) should be carried out for various angles of attack. For cases with vortex breakdown the unsteady flowfield has to be analysed. Important details related to numerical calculations are the position of the onset of vortex breakdown relative to the wing and the frequency of the surface pressure fluctuations in the vortex breakdown region.
8) Important parameters for the investigations according to 1) to 7) are the Reynolds number and the Mach number. A wide range for both parameters should be covered. Concerning the Reynolds number the fully laminar case at $R \cong 10^6$ should mark the lower end and the investigations should be extended to Reynolds numbers as high as possible. Concerning the Mach number incompressible flow should be included. In compressible flows with local supersonic zones the positions of the crossflow and terminating shocks should be determined experimentally, and in the vortex breakdown investigations according to 7) the interference between shock-induced pressure gradients and vortex breakdown location should be analysed.
9) The measurements according to 1) to 8) should also be extended to pitching and rolling slender wings. In cases with vortex breakdown time-accurate pressure distribution measurements should be carried out in order to separate the unsteadiness due to the wing motion from the unsteadiness caused by vortex breakdown.
10) The investigations according to 1) to 9) should be carried out for a wing with sharp leading edges as well as for at least one wing with rounded leading edges.

The experimental program sketched in these 10 paragraphs is a very comprehensive task, which can only be carried out by an international effort. In the following section some experimental techniques are described which might be suitable for the needed measurements, and in the final chapter a proposal for the model geometry and the organisation of an international program will be given.

5 Available experimental techniques

For all wind tunnels measurements of overall forces and moments by means of a sting-mounted strain gauge balance as well as pressure distribution measurements by surface pressure taps are standard techniques, which will not be treated separately. If high speed data acquisition in combination with a proper calibration of the lengths of the pressure tubes is applied, unsteady pressure distributions can also be measured. Some experimental techniques are available only in some wind tunnels. They will be described subsequently.

5.1 Hot-wire measurement technique (HWT)

The hot-wire technique is well known since a long time [42], and its main application lies in boundary layer measurements. However, this technique has also been successfully applied to vortical flowfields [26], [43], [44], [45], [46]. Usually cross-wire probe configurations are used, and for the determination of all three velocity components including the corresponding fluctuations, the probe has to be rotated around its axis by 90° to adjust the wire plane, and two traverse sweeps through the flowfield are necessary. If triple-wire probes are used all velocity components can be obtained in one sweep. The calibration and evaluation procedures are described in [45]. The hot-wire technique is a vulnerable tool since the probes can easily be destroyed by particles in the flowfield. Nevertheless this technique has been successfully applied to investigate very large vortical flowfields [26], [44], [45], [46] around delta wings, canard configurations and forward swept wings. An example taken from [26] is presented in Fig. 14. Concerning the needs for future experimental investigations it can be

expected that this experimental technique will bring about boundary layer measurements with distributions of velocities, turbulent kinetic energy and eddy viscosity. The hot-wire technique is also well suited for studies of the shear layer and the viscous core of the primary vortex as well as of the secondary and tertiary vortex regions.

5.2 Laser-Doppler Velocimetry (LDV)

Today many wind tunnels are equipped with a Laser-Doppler Velocimeter (LDV) for the non-intrusive measurement of all three velocity components and the six Reynolds stresses. These systems use lasers as the source of light in both forward and backward scattering mode. The forward scattering mode provides a higher signal to noise ratio, but it is not always applicable due to the arrangement of the model in the test section. In most systems three wavelengths of the laser light are used, and these three beams are divided into pairs by a network of beam-splitters and mirrors. The three pairs of beams are then focused in a small probe volume where they form three overlapping fringe works oriented at different angles with respect to the wind tunnel axis. For a single particle passing the three fringe patterns three instantaneous velocity components are acquired simultaneously. By means of Bragg cells as acoustic-optic modulators in each pair of beams, the flow direction can also be determined. Using statistical methods, the mean velocity component in each of the three directions as well as the Reynolds stresses are then calculated from a large number of particle signals.
The LDV technique as a non-intrusive method for unsteady flows, which provides the mean values as well as the fluctuations of all velocity components, has been applied to the vortical flow over delta wings, especially in studies of vortex breakdown [47], [48], [49], [50], [51], [52], [53], [54], [55]. An example taken from [55] is shown in Fig. 15.
This technique is well suited for the analysis of the structure of the flowfield especially in vortex sheets and in the primary vortices. If boundary layers as well as secondary and tertiary vortices are concerned, reflections from the wall have to be omitted and the movements of the probe volume relative to the wall have to be considered. Applications of the LDV technique in measurements of the surface shear stress will be discussed in section 5.6.5.

5.3 Particle Image Velocimetry (PIV)

In this technique the beam of a pulsed laser is formed into a light sheet. Particles added to the flow are illuminated and their scattered light exposes a photographic film or a CCD sensor [56], [57]. In laser sheet imaging (LSI) the particles just mark discrete stream filaments in order to make them visible and to yield qualitative information on the flow structure. In particle image velocimetry (PIV) the position of particles is determined at successive instants in order to gain quantitative informations on the local fluid motion. Concerning the flow around a delta wing the two instantaneous velocity components can be determined in one plane perpendicular to the main stream using commercial PIV systems. In order to get also the third velocity component in this plane the stereo technique has to be applied or two parallel light sheets (dual plane PIV) have to be considered. Full 3D flow surveys can be carried out by scanning the flowfield or by applying holographic PIV. These extended techniques are presently under development.
Particle image velocimetry has been applied to the flow around delta wings in [30], [58], [59], [60] as well as in [61], [62], [63]. An application of the stereo technique to a vortical flow is given in [64] and a result is shown in Fig. 16. Particle image velocimetry is a powerful tool for the investigation of the structure of vortical flows, but it is still a question

how close to a wall measurements can be carried out in order to investigate boundary layers and secondary and tertiary vortices.

5.4 Doppler global velocimetry (DGV)

In this technique a Laser light sheet is used which illuminates the flowfield in a cross section perpendicular to the main stream. The scattered light from the particles passes a filter with a permeability, which depends on the Doppler frequency. This means that at a certain point in the flowfield the velocity component in the direction of view is transformed into the brightness of the scattered light, which can be calibrated and measured. If the whole light sheet is considered, a global picture of this velocity component is established [65], [66], [67], [68], [69], [70], but one has to bear in mind that for a fixed camera position the direction of view is different for each point of the light sheet. Three velocity components can be obtained either by simultaneous viewing with three cameras from different positions in space or by means of a single camera at a fixed position and applying three different directions of the Laser light within the light sheet [67]. In the latter case the three velocity components are taken subsequently and the data do not belong to the same period of time. Up to now a single application on a delta wing has been published [66].

5.5 Pressure Sensitive Paint (PSP)

Pressure sensitive paint (PSP) is an efficient technique for measuring the surface pressure distribution on models without a large number of pressure taps. Pressure sensitive paints comprise a luminescent compound, which is stimulated by the absorption of light, and due to non-radiative processes such as oxygen quenching the wavelength of the emitted light is larger than that of the excitation. The intensity of the luminescence is correlated with the partial pressure of oxygen and hence with the ambient pressure.
PSP measurements are temperature sensitive. In a typical situation an error of 1 mb is induced by a temperature change of 0.1 K. A common way to correct for the temperature effects is to use some conventional pressure taps in order to calibrate the paint during the test assuming a uniform temperature distribution on the model. Apart from this low temperature-sensitive paints are needed.
The PSP technique is available since about 10 years [71], [72], [73], [74], [75]. Some papers contain measurements on delta wings [76], [77], [78]. Results for a double delta wing [79] are shown in Fig. 17, and the latest developments comprise the application on slender wings in unsteady motion [80], [33]. The present state of the art is described in [88]. By means of PSP detailed pressure distributions can be determined without a complicated wind tunnel model with a large number of pressure taps in positions, which have to be prescribed a priori.

5.6 Measurements of the Wall Shear Stress

For the validation of numerical results the magnitude and the direction of the local shear stress on the surface of the wing are needed.

5.6.1 Oil film interferometry

The classical method for an overview is the well-known oilflow pattern technique according to Figs. 5 and 6 which show the direction of the local wall shear stress. In many wind tunnels, especially for low speeds, this technique can easily be applied and even quantitative evaluations by means of the oil film interferometry [81], [82], [83], [84], [85], [86] are possible. Laser interferometry is used to measure the thinning rate of the oil film at a certain station and the shear stress is evaluated from the thin-oil-film equation. In recent improvements this technique has been extended to lines of oil, to multiple oil drops and to a technique in which multiple interferograms are acquired in a single run. Using these techniques 3D flows with high shear gradients can be investigated [87]. The state of the art is described in [88], and applications on delta wing flows are possible.
The oilfilm interferometry can also be used for the detection of transition on a wing since the sudden increase of the wall shear stress marks the onset of turbulent flow [88].

5.6.2 Floating element balance

In some wind tunnels the oil film interferometry cannot be applied since the test section is not accessible because it is pressurized and/or filled with another gas as in cryogenic wind tunnels. In such a situation local wall shear stress measurements could be carried out by all the well-known techniques [81] and using elements distributed in a certain pattern on the wing surface. Floating element balances measure the shear stress almost directly by means of one- or two-component balances, but at present the size of these elements is too large in order to determine the shear stress in a certain point. Progress in this field can be expected from micromachined wall shear stress sensors.

5.6.3 Pressure probes

Other sensors such as Preston tubes, surface fences and related devices [81], [82] could also be applied. In order to determine the direction of the shear stress the sensor elements should be turnable around an axis perpendicular to the wing surface. Unfortunately these sensors are not very sensitive with respect to the flow angle and therefore the accuracy of the measured flow directions is low. The sensors have to be calibrated and this might be a problem in wind tunnel applications.

5.6.4 Wall (pulsed) hot wires

In these methods the velocity is measured in a certain point located very close to the wall, and based on this velocity the wall shear stress is evaluated from v. Driest's law of the wall. Its shape is determined from a calibration, and the measured wall shear stresses are as good as the velocity distribution within the unknown boundary layer fits with that of the calibration. The velocity measurement can be carried out by means of a calibrated hot wire probe or by a calibrated pulsed hot wire probe. In order to determine also the direction of the shear stress the sensor elements have to be installed turnable around an axis perpendicular to the wall.

5.6.5 Wall-gradient LDV

The velocity near the wall can also be measured by LDV. In order to avoid vibrations of the Laser system relative to the wall the Laser system should be fixed to the wall. If parallel fringes are used the Doppler signals vary with the distance of the probe volume from the wall. If, however, a conical fringe system with its apex at the wall is used, the Doppler signals are the same for all distances of the probe volume from the wall, since in the viscous sublayer the velocity varies linearly with the distance from the wall. Thus such a Laser system measures the velocity gradient directly, and no calibration is necessary to evaluate the wall shear stress.

5.6.6 Other methods

The methods according to the sections 5.6.2 to 5.6.5 have not yet been applied to delta wing flows and they have been mentioned for the sake of completeness as possibilities to gain a limited number of data for comparison with numerical results. Two other methods namely the hot film technique and the liquid crystal technique are very important for wall shear stress measurements. Since they are also applicable in other respects they are treated in separate sections 5.7 and 5.8.

5.7 Hot film techniques

For heated surface elements the convective heat transfer is correlated with the wall skin friction. As in hot wire anemometry the constant current and the constant temperature modes are applied. The surface hot film elements can be used for the detection of transition without calibration, but for the evaluation of the wall shear stress they have to be calibrated [89], [90]. The resulting calibration curves are empirical functions between the heating voltage at the Wheatstone bridge and the wall shear stress. They depend on many flow parameters, and the reference flow for these calibrations is the main problem. Concerning hot film arrays the thermal interference amongst the hot films, caused by the temperature wake of an upstream hot film influencing the thermal boundary conditions of the downstream sensor, has to be taken into account. This interference can be eliminated by staggering the hot film sensors. If at a fixed position on the wing a V-shaped installation of two hot films is used, the direction of the local shear stress can be determined from the difference of the signals from both sides. The present status related to this technique is described in [88].
Hot film sensors and hot film arrays are widely used in wind tunnels for the detection of the laminar/turbulent boundary layer transition and of the onset of separation [90], [91], [92]. The use of this technique under cryogenic conditions is possible [93]. Up to now there exists just one application on delta wing flows [94].

5.8 Liquid crystal techniques

Another technique for wall shear stress measurements is the shear-sensitivity liquid crystal coating method [88], [95], [96], [97] which can be used for visualization and measurement of continuous surface shear stress vector distributions. White light illuminates the coated surface and if the reflected light is registered at a certain angle, a colour change is observed if the shear stress has a component in the direction of view. A calibration colour vs shear is required and the reference shear has to be measured by another method such as hot film or oil

drop interferometry. In order to evaluate also the direction of the shear stress, a certain point is viewed from different directions and a Gaussian curve fit is used for the determination of the vector orientation. Up to now the method described so far is confined to plane surfaces.
Using temperature sensitive liquid crystal coating the surface temperature distribution can also be measured after a calibration colour vs temperature. For this kind of liquid crystals the fluid matrix has been replaced by plastic foils. Progress in wall shear stress measurements for arbitrarily shaped bodies can be expected from the application of such foils for liquid crystal coating.

5.9 Piezoelectric foil arrays

Piezo sensor arrays are made of a plastic foil with piezo- and pyroelectric properties: Electrical surface charges are caused by mechanical pressure as well as by temperature changes within the material. If a small temperature gradient between sensor and fluid is used, the pyroelectric properties of the foil are predominant and high signal to noise ratios are achieved. For this purpose piezo foils are heated, and the wall shear stress fluctuations are determined from the heat flux fluctuations by means of the Reynolds analogy.
Piezo foils are mainly used for the detection of transition in wind tunnels as well as in free flight [98], [99], [100]. The present state of this technique is summarized in [88]. Applications on slender delta wings have not yet been performed

5.10 Infrared technique

The wall temperature can be measured by means of an infrared camera, which is calibrated against some surface mounted thermocouples. The same can be achieved by means of temperature sensitive paint according to section 5.5. The magnitude of the local wall shear stress is related to the heat flux through the Reynolds analogy. Sudden jumps in local surface temperature might indicate laminar/turbulent boundary layer transition, but high heat transfer rates can also be generated by high velocities underneath the vortices on a delta wing. Therefore the pressure distribution has a significant influence and both effects cannot be separated definitely. Progress can be expected from a combination of the PSP method for the determination of the pressure or the local velocity at the outer edge of the boundary layer and the infrared technique for the determination of the heat flux.

6 Proposal for a new vortex flow experiment (VFE-2)

The flow around a slender delta wing and the needs for further experimental data for the validation of numerical methods have been described in section 4, and the available experimental techniques are summarized briefly in section 5. Following here the configuration for a new vortex flow experiment and the program for new measurements will be discussed.

6.1 Geometry of the configuration

The planform of the configuration should be chosen in such a way that all flow regimes, which occur with increasing angle of attack, are covered properly. The main parameter for

this is the aspect ratio or the leading-edge sweep of the wing, and for a leading-edge sweep of 65°, corresponding to an aspect ratio A = 1.85, the flow regimes are established as follows

i) Attached flow without vortex formation $0° \leq \alpha \leq 4°$
ii) Separated vortical flow without vortex breakdown $4° \leq \alpha \leq 20°$
iii) Separated vortical flow with vortex breakdown $20° \leq \alpha \leq 40°$
iv) Separated deadwater-type flow $40° \leq \alpha \leq 90°$.

This favourable partitioning of the angle of attack range is the reason why 65° swept wings have been chosen for the VFE-1 [1], [2], at NASA [15] and at NAE [31]. The VFE-1 wing is the only one with cropped wing tips. Since the grid generation technique for numerical methods is well established, pointed wing tips are no problem and therefore a simple delta wing with 65 ° leading edge sweep can be chosen.

Concerning the thickness distribution a sharp as well as some (at least one) rounded leading edges should be chosen. Camber and twist should not be applied. In order to fix the model at a rear sting a symmetrical fuselage is necessary, but it should be kept as small as possible in order to minimize the deviation from a simple delta wing.

All these requirements are fulfilled by the NASA configuration [15], which is shown in Figs. 18 and 19. Its data are

Leading-edge sweep	$\Lambda = 65°$
Aspect ratio	$A = 1.85$
Mean aerodynamic chord ratio	$\bar{c} / c_R = 2/3$
Flat plate thickness ratio	$t / c_R = 0.034$
Streamwise leading-edge radii	$r_{LE} / \bar{c} = 0$
	$= 0.0005$
	$= 0.0015$
	$= 0.0030$.

The wing consists of an inner flat plate part and interchangeable leading edges with four different leading-edge radii as well as a trailing-edge closure region. The wing geometry is described by means of analytical expressions. In the rear part of the wing a small sting fairing is applied and its shape is also given by analytical expressions. In addition the geometry of the model sting is described in all details in [15].

To apply this wing as the basic configuration for a new vortex flow experiment has the following advantages:

i) If a new wind tunnel model shall be built, the geometry of the wing and the sting are available in analytical form and the manufacture of the model is easy.
ii) For all four configurations of this delta wing the overall aerodynamic coefficients as well as the pressure distributions in sections at $x / c_R = 0.2; 0.4; 0.6; 0.8$ and 0.95 are available in [15] for a large variety of Reynolds numbers and Mach numbers. These data can be chosen for comparison with those of the first wind tunnel entry of the new model.

6.2 Test program

For comparison with numerical results the following experiments should be carried out:

1) Detection of transition laminar/turbulent.
2) Detailed pressure distribution measurements.
3) Boundary layer measurements including total pressure, components of velocity and vorticity, turbulent energy and eddy viscosity.

4) Determination of the wall shear stress and detection of the secondary and tertiary separation lines.
5) Flowfield measurements in the primary and secondary vortices including total pressure, components of velocity and vorticity, turbulent energy and eddy viscosity.

Measurements of this kind should be carried out in a wide angle of attack range. In the regime without vortex breakdown the angle of attack should be chosen as high as possible in order to investigate cases with large vortical effects.
In the regime with vortex breakdown the additional analysis of the unsteady flow should lead to the

6) Position of the onset of vortex breakdown from flowfield measurements and to the
7) Frequency of the surface pressure fluctuations in the vortex breakdown region.

All investigations should be carried out for

8) Various Reynolds numbers, starting with the fully laminar case at $R \cong 10^6$ up to Reynolds numbers as high as possible.
9) Various Mach numbers. The incompressible case should be included. For compressible flows with local supersonic zones the positions of the crossflow and terminating shocks should be determined experimentally, and in cases with vortex breakdown the interference between shock-induced pressure gradients and vortex breakdown location should be analyzed.

Concerning unsteady boundary conditions the configuration according to section 6.1 should also be tested in

10) Pitching and rolling motion. In cases with vortex breakdown time-accurate pressuredistribution measurements should be carried out in order to separate the unsteadiness due to the wing motion from the unsteadiness caused by vortex breakdown.

The investigations mentioned so far should be carried out for the wing with

11) Sharp and (at least one) rounded leading edge.

6.3 Organization of the new vortex flow experiment (VFE-2)

Experimental data as well as numerical results for the proposed configuration are highly welcome. Results should be published and corresponding data files should be made available for the scientific community through a web-site as in [15]. Short notes on the existence of a publication and a web-site should be sent to the authors at DLR (Guenter.Redeker@dlr.de). From time to time a status report on the VFE-2 will be published and if appropriate a symposium will be arranged.

7 Summary

The vortex formation on the upper surface of slender wings is described in some detail and the interference mechanisms between primary and secondary vortices as well as the vortex breakdown phenomenon are especially emphasized. The effects of Mach number and Reynolds number are treated separately for sharp and rounded leading edges. The experimental details necessary for the validation of numerical methods are derived and a brief review of relevant modern experimental techniques is given. Finally a configuration suited for a new International Vortex Flow Experiment (VFE-2) as well as a corresponding test program and a handling procedure are presented.

8 Acknowledgements

The authors would like to thank Ch. Breitsamter, TU München, W. Fritz, EADS München, Th. Löser, DNW Braunschweig, J.M. Luckring, NASA Langley Research Center, A.T. Mitchell, USAF Academy Colorado and J. Müller, Volkswagen AG Wolfsburg, for the submission of the drawings from their original publications. In addition the various discussions with the DLR experimental team of K.-A. Bütefisch, R.H. Engler, J. Kompenhans and H.-P. Kreplin and with A. Bergmann, DNW Braunschweig, are gratefully acknowledged.

9 References

[1] Drougge, G.: The international vortex flow experiment for computer code validation. ICAS-Proceedings 1988, Vol. 1, pp. XXXV-XLI.

[2] Elsenaar, A.; Hjelmberg, L.; Bütefisch, K.-A. and Bannink, W.J.: The international vortex flow experiment. AGARD-CP 437 (1988), Vol.1, pp .9-1 to 9-23.

[3] Wagner, B.; Hitzel, S.; Schmatz, M.A.; Schwarz, W.; Hilgenstock, A. and Scherr, S.: Status of CFD validation on the vortex flow experiment. AGARD-CP 437 (1988), Vol. 1, pp. 10-1 to 10-10.

[4] Hoeijmakers, H.W.M.: Modelling and numerical simulation of vortex flow in aerodynamics. AGARD-CP 494 (1991), pp. 1-1 to 1-46.

[5] Luckring, J.M.: Recent progress in computational vortex-flow aerodynamics. AGARD-CP 494 (1991), pp. 6-1 to 6-21.

[6] Hilgenstock, A. and Vollmers, H.: On the simulation of compressible turbulent flows past delta wing, delta wing-body and delta wing-canard. AGARD-CP 494 (1991), pp.7-1 to 7-13.

[7] Williams, B.R.; Kordulla, W.; Borsi, M. and Hoeijmakers, H.W.M.: Comparison of various Euler solvers and one Navier-Stokes solver for the flow about a sharp-edged cropped delta wing. AGARD CP-494 (1991), pp. 2-1 to 2-12.

[8] Borsi, M.; Kordulla, W.; Hoeijmakers, H.W.M. and Williams, B.R.: Comparison of solution of various Navier-Stokes solvers and one Euler solver for the flow about a sharp edged cropped delta wing. In: Royal Aeron. Soc. (Ed.): Proceedings of the 1993 European Forum on “Recent Developments and Applications in Aeronautical CFD”, Bristol 1993, pp. 5.1 - 5.11.

[9] Baldwin, B.S. and Lomax, H.: Thin layer approximation and algebraic model for separated turbulent flows. AIAA Paper 78-257 (1978).

[10] Degani, D. and Schiff, L.B.: Computation of turbulent supersonic flows around pointed bodies having crossflow separation. J. Comp. Physics 66 (1986), 173 – 196.

.

[11] Wilcox, D.C.: Turbulence modelling for CFD. 2nd Ed., DCW Industries, Inc. (1998).

[12] Hummel, D.: Zur Umströmung scharfkantiger schlanker Deltaflügel bei großen Anstellwinkeln. Z. Flugwiss. 15 (1967), 376 – 385.

[13] Smith, J.H.B.: Improved calculations of leading-edge separation from slender delta wings. RAE TR 66070 (1966).

[14] Hummel, D.: Experimentelle Untersuchung der Strömung auf der Saugseite eines Deltaflügels. Z. Flugwiss. 13 (1965), 247 – 252.

[15] Chu, J. and Luckring, J.M.: Experimental surface pressure data obtained on 65° delta wing across Reynolds number and Mach number ranges. NASA TM 4645 (1996).

[16] Erickson, G.E.: Wind tunnel investigation of the interaction and breakdown characteristics of slender-wing vortices at subsonic, transonic, and supersonic speeds. NASA TP 3114 (1991).

[17] Werlé. H.: Sur l'éclatement des tourbillons d'apex d'une aile delta aux faibles vitesses. La Recherche Aéronautique 74 (1960), 23 – 30.

[18] Lambourne, N.C. and Bryer, D.W.: The bursting of leading edge vortices. Some observations and discussion of the phenomenon. ARC R & M 3282 (1962).

[19] Ekaterinaris, J.A. and Schiff, L.B.: Numerical simulation of incidence and sweep effects on delta wing vortex breakdown. J. Aircraft 31 (5) ,1994, 1043 –1049.

[20] Visbal, M.R.: Computed unsteady structure of spiral vortex breakdown on delta wings. AIAA Paper 96-2074 (1996).

[21] Gordnier, R.E.: Computational study of a turbulent delta-wing flowfield using two-equation turbulence models. AIAA Paper 96-2076 (1996).

[22] Müller, J. and Hummel, D.: Time-accurate CFD analysis of the unsteady flow on a fixed delta wing. AIAA Paper 2000-0138 (2000).

[23] Murayama, M.; Nakahashi, K. and Sawada, K.: Numerical simulation of vortex breakdown using adaptive grid refinement with vortex-center identification. AIAA Paper 2000-0806 (2000).

[24] Müller, J. and Hummel, D.: Numerical analysis of the unsteady flow above a slender delta wing at large angles of attack. ICAS Proceedings 2000, Paper ICA0252 (2000).

[25] Gursul, I.: Unsteady flow phenomena over delta wings at high angle of attack. AIAA J. 32 (2), 1994, 225 – 231.

[26] Breitsamter, C.: Turbulente Strömungsstrukturen an Flugzeugkonfiguratione mitVorderkantenwirbeln. Thesis TU München, Herbert Utz Verlag Wissenschaft (1997).

[27] Huang, X.Z.; Jobe, C.E. and Hanff, E.S.: A critical assessment and requirement for ground testing on vortex breakdown locations over delta wings. RTO/AVT Symposium Loen, Norway, May 2001, Paper 17.

[28] Thomer, O.; Krause, E. and Schroeder, W.: Normal shock vortex interaction. RTO/AVT Symposium Loen, Norway, May 2001, Paper 18.

[29] Hummel, D. and Löser, Th.: Low speed wind tunnel experiments on a delta wing oscillating in pitch. ICAS Proceedings 1998, Paper ICAS-98-3.9.3.

[30] Neuwerth, G.; Peiter, U.; Decker, F. and Jacob, D.: Reynolds number effects on the low-speed aerodynamics of the hypersonic configuration ELAC-1. AIAA Paper 98-1578 (1998)

[31] Huang, X.Z.; Hanff, E.S.; Jenkins, J.E. and Addington, G.: Leading-edge vortex behavior on a 65 °delta wing oscillating in roll. AIAA Paper 94-3507 (1994).

[32] Löser, Th.: Dynamic force and pressure measurements on an oscillating delta wing at low speeds. DLR IB 129-96/9 (1996).

[33] Engler, R.; Fonov, S.; Klein, Ch.; Bütefisch, K.-A.; Bock, K.-W.; Weiskat, D. and Fritz, W.: Study on unsteady vortex behavior of a rotating 65° delta wing at M = 0.8 using pressure sensitive paint (PSP). RTO/AVT Symposium Loen, Norway, May 2001, Paper 6.

[34] Visbal, M.R.: Onset of vortex breakdown above a pitching delta wing. AIAA J. 32 (8), 1994, 1568 – 1575.

[35] Fritz, W.: Unsteady Navier Stokes calculations for a delta wing oscillating in pitch. ICAS Proceedings 1998, Paper ICAS-98-2.4.1 (1998).

[36] Arthur, M.T.; Brandsma, F.; Ceresola, N. and Kordulla, W.: Time accurate Euler calculations of vortical flow on a delta wing in pitching motion. AIAA Paper 99-3110 (1999).

[37] Gordnier, R.E. and Visbal, M.R.: Numerical simulation of delta-wing roll. AIAA Paper 93-0554 (1993).

[38] Gordnier, R.E.: Computation of delta-wing roll maneuvers. AIAA Paper 93-2975 (1993).

[39] Chaderjian, N.M. and Schiff, L.B.: Navier-Stokes predictions of delta wing in roll with vortex breakdown. AIAA Paper 93-3495 (1993).

[40] Fritz, W.; Arthur, M.T.; Brandsma, F.J.; Bütefisch, K.-A. and Ceresola, N.: Time accurate Euler calculations of vortical flow over a delta wing in rolling motion. RTO/AVT Symposium Loen, Norway, May 2001, Paper 11.

[41] Hummel, D.: Experimentelle Untersuchung dreidimensionaler laminarer Grenzschichten an einem schlanken Deltaflügel. Z. Flugwiss. Weltraumforsch. 10 (1986), 133 – 145.

[42] Lomas, C.G.: Fundamentals of hot wire anemometry. Cambridge Univers. Press London 1986.

[43] Visser, K.D. and Nelson, R.C.: Measurements of circulation and vorticity in the leading-edge vortex of a delta wing. AIAA J. 31 (1), 1993, 104 – 111.

[44] Breitsamter, C. and Laschka, B.: Velocity measurements with hot-wires in a vortex-dominated flowfield. AGARD-CP 535 (1993), pp. 11-1 to 11-13.

[45] Laschka, B.; Ranke, H. and Breitsamter, C.: Application of unsteady measurement techniques to vortical and separated flows. Z. Flugwiss. Weltraumforsch. 19 (1995), 90 – 108.

[46] Breitsamter, C. and Laschka, B.: Vortical flowfield structure at forward swept wing configurations. ICAS Proceedings 1998, Paper ICAS-98-3.8.2.

[47] Elsenaar, A. and Bütefisch, K.-A.: Experimental study on vortex and shock wave development on a 65° delta wing. IUTAM Symposium Transsonicum III, Göttingen, 1988, 281 - 290.

[48] Kjelgaard, S. O. and Sellers, W.L.: Detailed flowfield measurements over a 75° swept delta wing for code validation. AGARD-CP 437 (1988), Vol. II, P10-1 to P10-14.

[49] Kegelman, J.T. and Roos, F.W.: Effects of leading-edge shape and vortex burst on the flowfield of a 70-degree-sweep delta wing. AIAA Paper 89-0086 (1989).

[50] Agrawal, S.; Barnett, R.M. and Robinson, B.A.: Numerical investigation of vortex breakdown on a delta wing. AIAA J. 30 (3), 1992, 584 – 591.

[51] Molton, P.: Etude expérimentale de l'éclatement tourbillonaire sur aile delta en écoulement incompressible. Caractérisation du champ externe. ONERA RT 53/1147AN (1992).

[52] Délery, J.: Aspects of vortex breakdown. Progress in Aerospace Sciences 30 (1994), 1 – 59.

[53] Pelletier, A. and Nelson, R.C.: Factors influencing vortex breakdown over 70 degree delta wings. AIAA Paper 95-3469 (1995).

[54] Mitchell, A.M.; Molton. P.; Barberis, D. and Délery, J.: Characterization of vortex breakdown by flow field and surface measurements. AIAA Paper 2000-0788 (2000).

[55] Mitchell, A.M.: Caractérisation et contrôle de l'éclatement tourbillonnaire sur une aile delta aux hautes incidences. Thèse de Doctorat de l'Université Paris VI. ONERA Note Technique 2000-6 (2000).

[56] Adrian, R.J.: Particle imaging techniques for experimental fluid mechanics. Ann. Rev. of Fluid Mech. 23 (1991), 261 – 304.

[57] Raffel, M.; Willert, C.E. and Kompenhans, J.: Particle image velocimetry – a practical guide. Springer-Verlag, 1998.

[58] Magness, C.; Robinson, O. and Rockwell, D.: Unsteady crossflow on a delta wing using particle image velocimetry. J. Aircraft 29 (4), 1992, 707 – 709.

[59] Dieterle, L.; Raffel, J.; Ehrenfried, K. and Kompenhans, J.: Flow measurements on a large delta wing using particle image velocimetry (PIV). Laser Symposium Lisbon, 1998.

[60] Dieterle, L.; Kompenhans, J.; Peiter, U. and Pengel, K.: Flow field investigations on a large wing using LSI and PIV. 8th International Symposium on Flow Visualization Sorrento, 1998.

[61] Brücker, C. and Althaus, W.: Study of vortex breakdown by particle tracking velocimetry (PTV). Part 1: Bubble type. Experiments in Fluids 13 (1992), 339 – 349.

[62] Brücker, C.: Study of vortex breakdown by particle tracking velocimetry (PTV). Part 2: Spiral type. Experiments in Fluids 14 (1993), 133 – 139.

[63] Brücker, C. and Althaus, W.: Study of vortex breakdown by particle tracking velocimetry (PTV). Part 3: Time-dependent structure and development of breakdown modes. Experiments in Fluids 16 (1995), 174 – 186.

[64] Willert, Ch.: Stereoscopic digital particle image velocimetry for application in wind tunnel flows. Meas. Sci. Technol. 8 (1997), 1465 - 1479.

[65] Komine, H.; Brosnan, S.J.; Litton, A.B. and Stappaerts, E.A.: Real-time Doppler global velocimetry. AIAA Paper 91-0337 (1991).

[66] Meyers, J.F.; Lee, F.W. and Cavone, A.A.: Three component Doppler global velocimetry measurements of the flow above a delta wing. Laser Techniques and Applications in Fluid Mechanics, Springer-Verlag, 1993, pp. 345 – 363.

[67] Roehle, I. and Schodl, R.: Evaluation of the accuracy of the Doppler global technique. Proc. Optical Methods and Data Processing in Heat and Fluid Flow, London, 1994, 155 – 161.

[68] Meyers, J.F.: Development of Doppler global velocimetry as a flow diagnostic tool. Meas. Sci. Technol. 6 (1995), 769 – 783.

[69] NASA (Ed.): Doppler global velocimetry. Development of a flight research instrumentation system for application to nonintrusive measurements of the flow field. NASA – CR-191490 (1994).

[70] McKenzie, R.L.: Planar Doppler velocimetry for large-scale wind tunnel applications. AGARD-FDP Symposium on Advanced Aerodynamic Measurement Technology, 1997, Paper No. 9.

[71] Engler, R.H.; Hartmann, K.; Troyanovski, I. and Vollan, A.: Description and assessment of a new optical pressure measurement system (OPMS) demonstrated in the high speed wind tunnel of DLR in Göttingen. DLR-FB 92-24 (1992).

[72] Morris,M.J.; Donovan, J.F.; Kegelman, J.T.; Schwab, S.D.; Levy, R.L. and Crites, R.C.: Aerodynamic applications of pressure sensitive paint. AIAA J. 31 (3), 1993, 419 – 425.

[73] Morris, M.J.: Use of pressure-sensitive paints in low-speed flows. ICIASF Congress 95. IEEE Publication 95CH3482-7 (1995).

[74] Engler, R.H. and Klein, C.: First results using the new DLR PSP system – intensity and lifetime measurements. Proceedings of the CEAS Wind Tunnels and Wind Tunnel Test Techniques Conference, Cambridge, 1997, Paper 43.

[75] Davies, A.G.: Recent developments in pressure sensitive paint measurements using the BAe system. Proceedings of the CEAS Wind Tunnels and Wind Tunnel Test Techniques Conference, Cambridge, 1997, Paper 28.

[76] Liu, T.; Campbell, B.T.; Burns, S.P. and Sullivan, J.P.: Temperature and pressure sensitive luminescent paints in aerodynamics. Appl. Mech. Review 50 (1997), No. 4.

[77] Baker, W.M.: Recent experiences with pressure sensitive paint testing. AIAA Paper 2001-0135 (2001).

[78] Le Sant, Y.; Bouvier, F.; Merienne, M.-C. and Peron, J.-L.: Low speed tests using PSP at ONERA. AIAA Paper 2001-0555 (2001).

[79] Klein, C. and Engler, R.H.: Visualization of aerodynamic effects on a double-delta wing aircraft model using pressure sensitive paint (PSP) technique. Journal of Visualization Vol. 2, No. 1, 1999, 9 – 16.

[80] Klein, C.: Einsatz einer druckempfindlichen Beschichtung (PSP) zur Bestimmung des momentanen Druckfeldes von Modellen im Windkanal. DLR-FB 97-55 (1997).

[81] Hartonidis, J.: The measurement of wall shear stress. In: M.G. el Hak (Ed.): Advances in Fluid Mechanics. Springer-Verlag 1989, 229 – 261.

[82] Fernholz, H.H.; Janke, G.; Wagner, P.M. and Warnack, D.: New developments and applications of skin-friction measuring techniques. Meas. Sci. Technol. 7 (1996), 1396 – 1409.

[83] Mateer, G.M.; Monson, D.J. and Menter, F.R.: Skin-friction measurements and calculations on a lifting airfoil. AIAA J. 34 (2), 1996, 231 – 236.

[84] Driver, D.: Applications of oil-film interferometry skin-friction technique to large wind tunnels. AGARD-CP 601 (1997), Paper 25.

[85] Schülein, E.; Kosh, S. and Rosemann, H.: Skin friction measurement and transition detection techniques for the Ludwieg-tubes at DLR. Proc. RTO/AGARD Fluid Dynamics Measurement Technology, Seattle 1997, 32-1 to 32-9 (1997).

[86] Naughton, J. and Sheplak, M.: Modern skin friction measurement techniques: Description, use and what to do with the data. AIAA Paper 2000-2521 (2000).

[87] Thomas, S.K. and Naughton, J.W.: Comparative analysis of thin-oil-film interferometric skin friction measurement techniques. AIAA Paper 2001-0558 (2001).

[88] Von Kármán Institute for Fluid Dynamics (Ed.): Lecture Series on Advanced Measurement Techniques, Brussels, 29 Jan to 1 Feb 2001. VKI Lecture Series 2001-01.

[89] Nitsche, W.; Haberland, C. and Thünkler, R.: Comparative investigations on skin friction measurement techniques in experimental aerodynamics. ICAS Proceedings 1984, Paper 84-2.4.1.

[90] Haselbach, F.: Thermalhaushalt und Kalibration von Oberflächenheißfilmen und Heißfilmarrays. VDI Fortschritts-Bericht, Reihe 7, Nr. 326 (1997).

[91] Kreplin, H.-P. and Höhler, G.: Application of the hot-film technique to laminar flow investigations. Proc. 1st European Forum on Laminar Flow Technology, Hamburg, Paper 92-01-017 (1992), DGLR-Bericht 92-06, 123 – 131.

[92] Nakayama, A.; Stack, J.P.; Lin, J.C. and Valazero, W.O.: Surface hot-film technique for measurements of transition, separation, and reattachment points. AIAA Paper 93-2918 (1993).

[93] Gartenberg, E.; Scott, M.A.; Matinson, S.D. and Tran, S.Q.: Boundary layer transition detection with hot-films in cryogenic wind tunnels. 4th Int. Symposium on Fluid Control, Measurement and Visualization, Toulouse, France (1994).

[94] Kuppa, S.; Mangalam, S.M.; Harvey, W.D. and Washburn, A.E.: Transition detection on a delta wing with multi-element hot-film sensors. AIAA Paper 95-1782 (1995).

[95] Reda, D.C. and Muratore, J.J., Jr.: Measurement of surface shear stress vectors using liquid crystal coatings. AIAA J. 32 (8), 1994, 1576 – 1582.

[96] Reda, D.C. and Wilder, M.C.: Quantitative and qualitative aspects of the shear-sensitive liquid crystal coating method. ICAS Proceedings 1998, Paper ICAS-98-3.3.2.

[97] Reda, D.C. and Wilder, M.C.: Shear-sensitive liquid crystal coating method applied through transparent test surfaces. AIAA J. 39 (1), 2001, 195 – 197.

[98] Nitsche, W.; Mirow, P. and Dörfler, T.: Application of piezoelectric foils in experimental aerodynamics. Proceedings of the ICIASF'89, Göttingen, 1991, 57 – 65.

[99] Ewald, B.; Durst, F.; Krause, E. and Nitsche, W.: In-flight measuring techniques for laminar flow wing development. Z. Flugwiss. Weltraumforsch. 17 (1993), 294 – 310.

[100] Nitsche, W. and Szodruch, J.: Laminar-flow instrumentation for wind-tunnel and flight experiments. J.Aircraft 30 (2), 1993, 192 – 200.

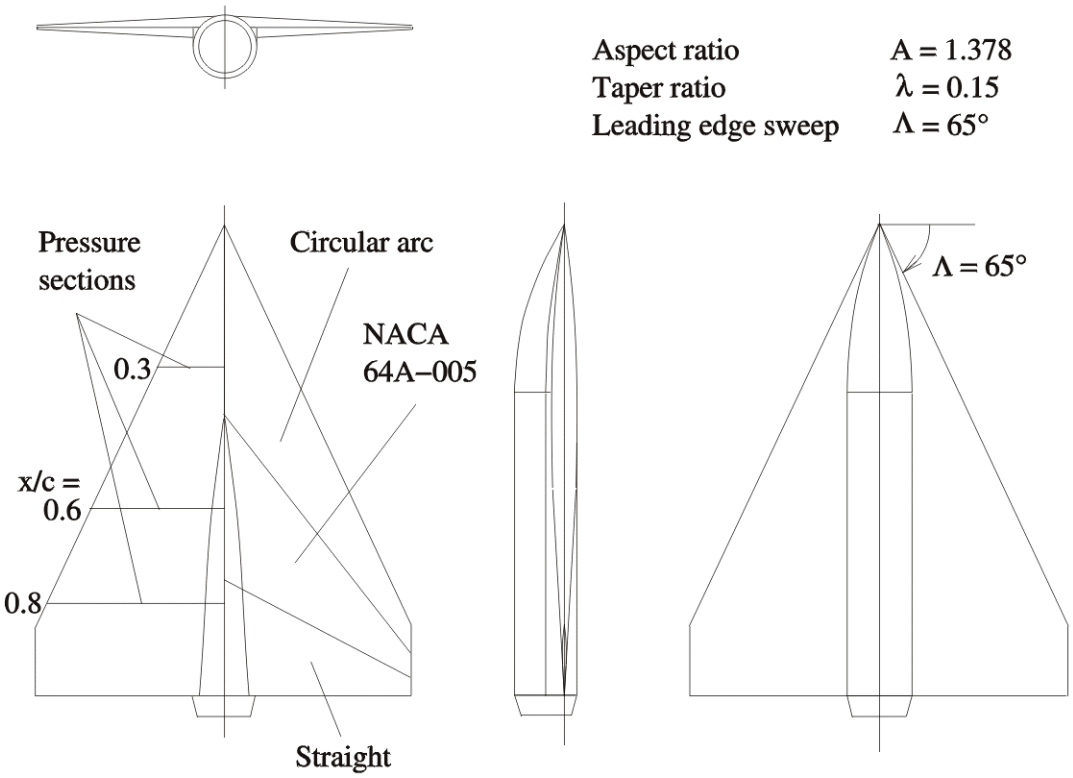

Fig. 1: Configuration of the International Vortex Flow Experiment (VFE-1)

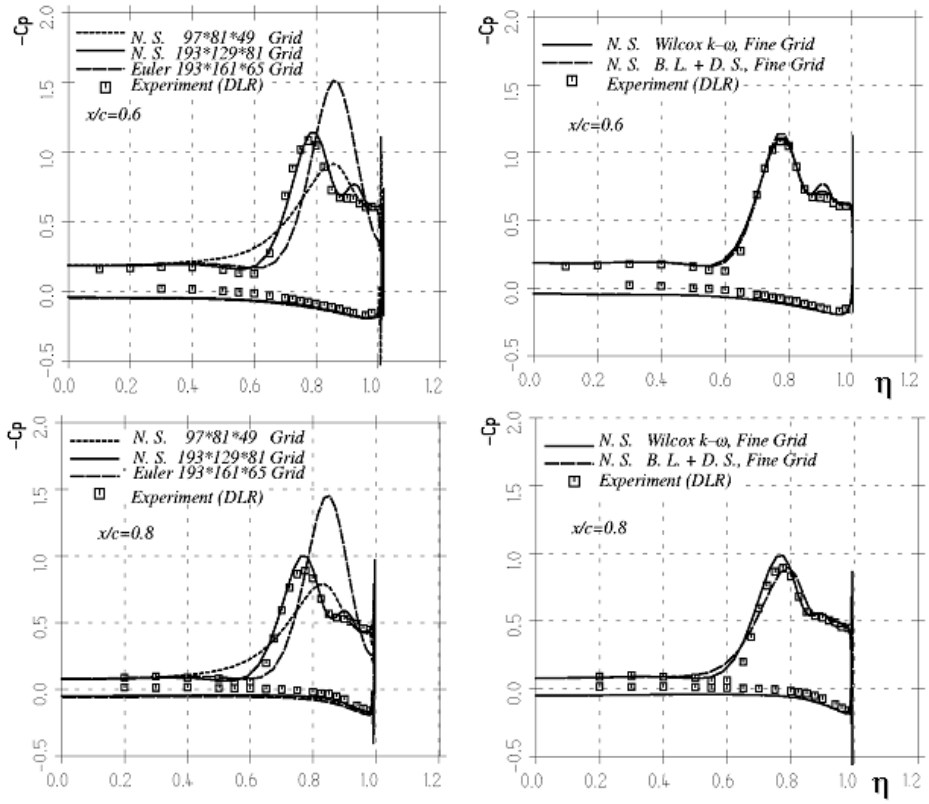

Fig. 2: Surface pressure distributions on the wing (only) of the VFE-1 configuration at M = 0.4, R = 3.1 • 10^6 , α = 9°. Effects of grid resolution and turbulence modelling. FLOWer code results according to W. Fritz, EADS Munich.

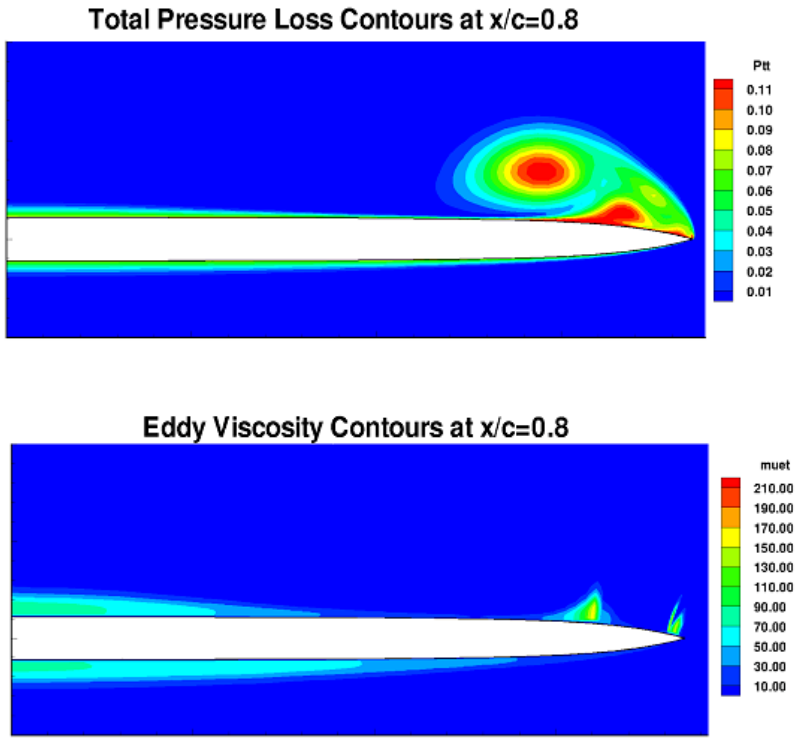

Fig.3: Total pressure loss and eddy viscosity contours in section x/c = 0.8 on the wing of the VFE-1 configuration at M = 0.4, R = 3.1 • 10^6, α = 9°. FLOWer code results using the Baldwin-Lomax turbulence model according to W. Fritz, EADS Munich

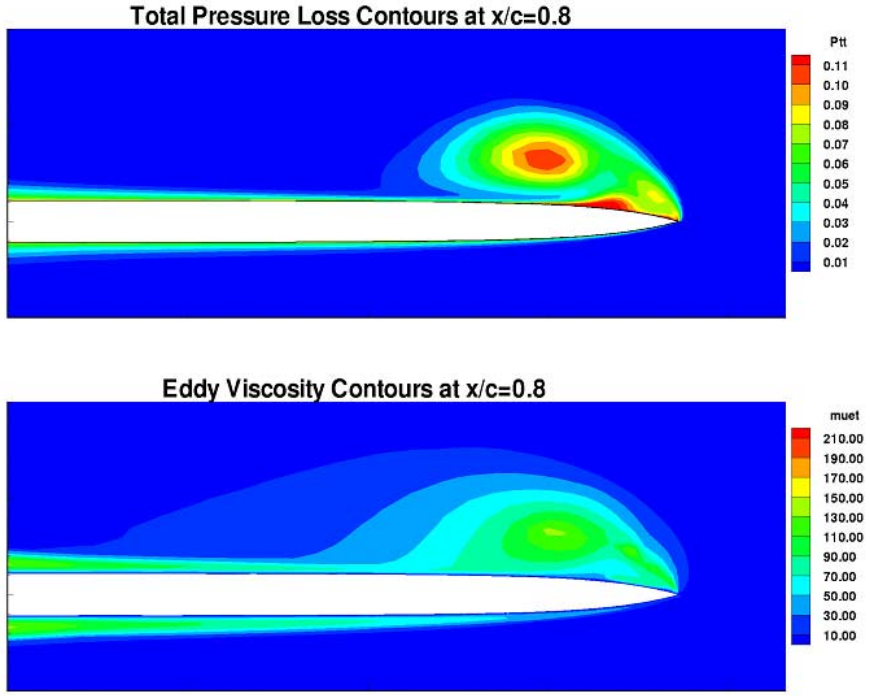

Fig. 4: Total pressure loss and eddy viscosity contours in section x/c = 0.8 on the wing of the VFE-1 configuration at M = 0.4, R = 3.1 • 10^6, α = 9°. FLOWer code results using the Wilcox k - ω turbulence model according to W. Fritz, EADS Munich

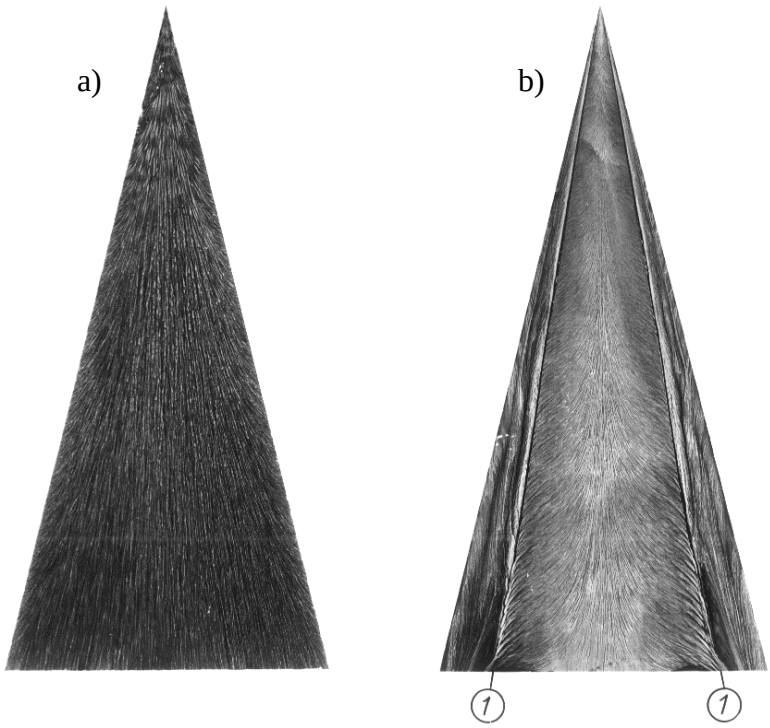

Fig. 5: Oilflow patterns on a delta wing A = 1.0 at R = 9 • 10^5, laminar boundary layers
a) α = 20.5°, pressure side
b) α = 20.5°, suction side
(1) Secondary separation line

Fig. 6: Oilflow patterns on a delta wing A = 1.0 at α = 20.5°, suction side with artificially turbulent boundary layers
(1) Secondary separation line
(2) Turbulence generator

Fig. 7: Pressure distribution and vortex formation on delta wing A = 1.0 at α = 20.5° in the section at x/c = 0.3

a) Pressure distribution

boundary layer

—●— laminar

—o— turbulent

– – – Theory J. H. B. Smith

b) Vortex formation (schematic)

boundary layer

—— laminar

– – – turbulent

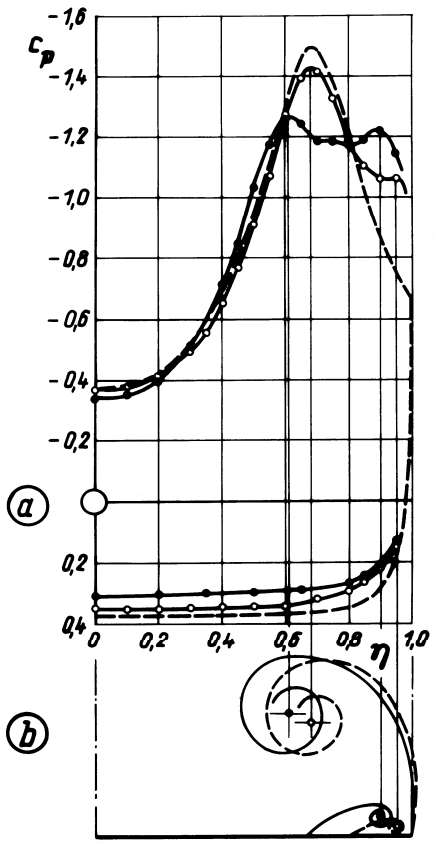

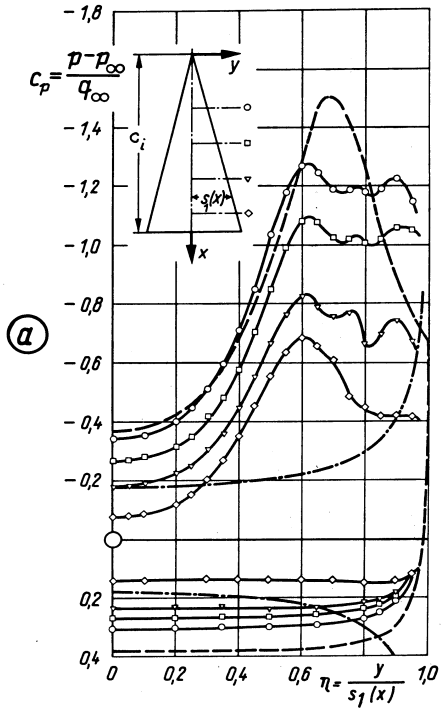

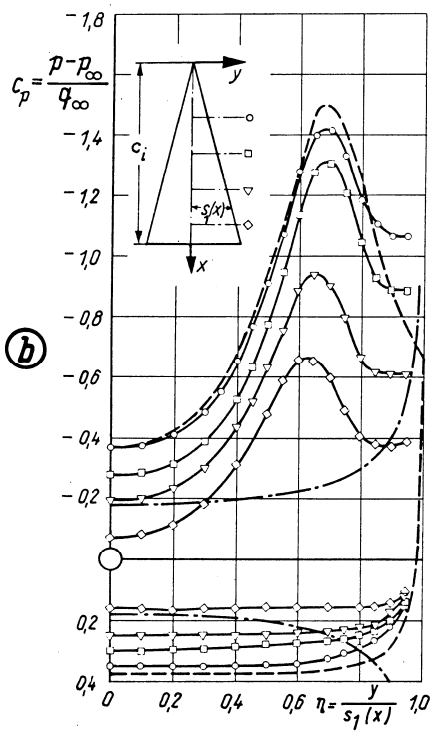

Fig. 8: Pressure distribution on delta wing A = 1.0 at α = 20.5°

a) Re = $9 \cdot 10^5$, laminar boundary layers

b) Artificially turbulent boundary layers

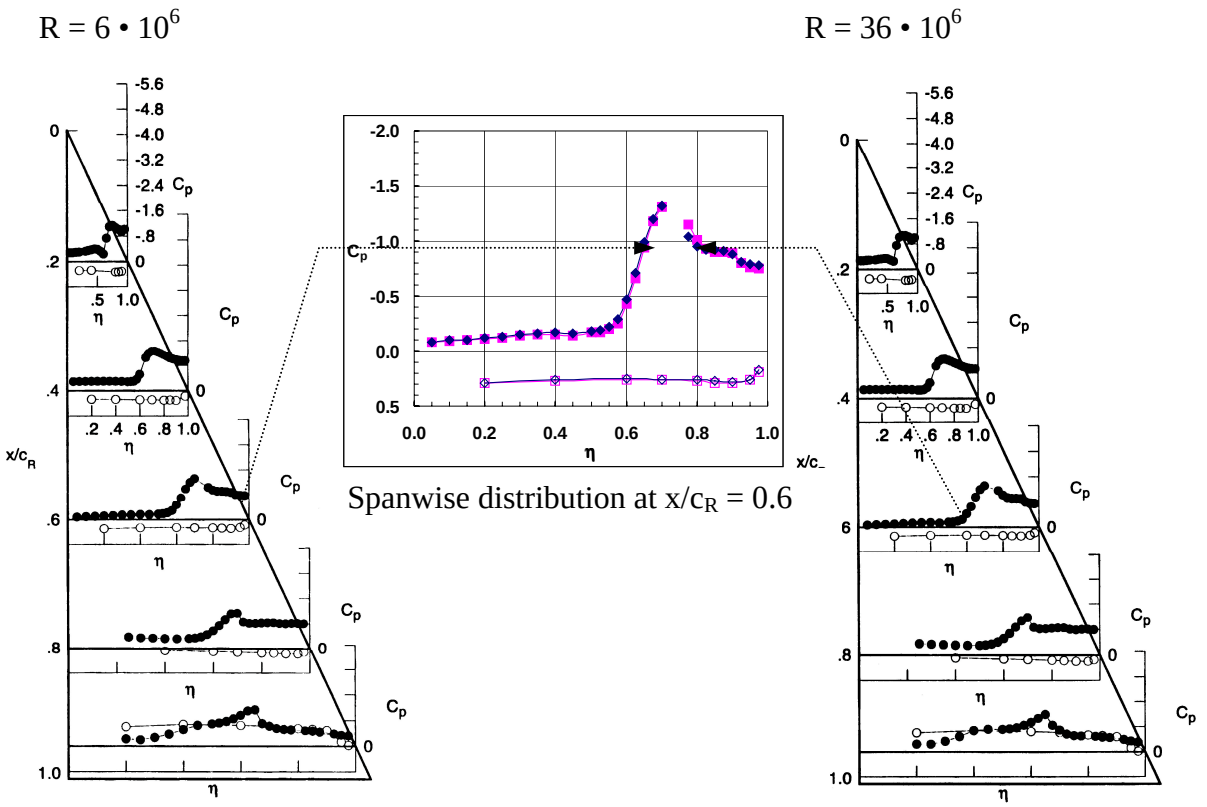

Fig. 9: Effect of Reynolds number on the pressure distribution of the A = 1.85 (Λ = 65°) sharp-edged delta wing at M = 0.85, α = 13° [15]

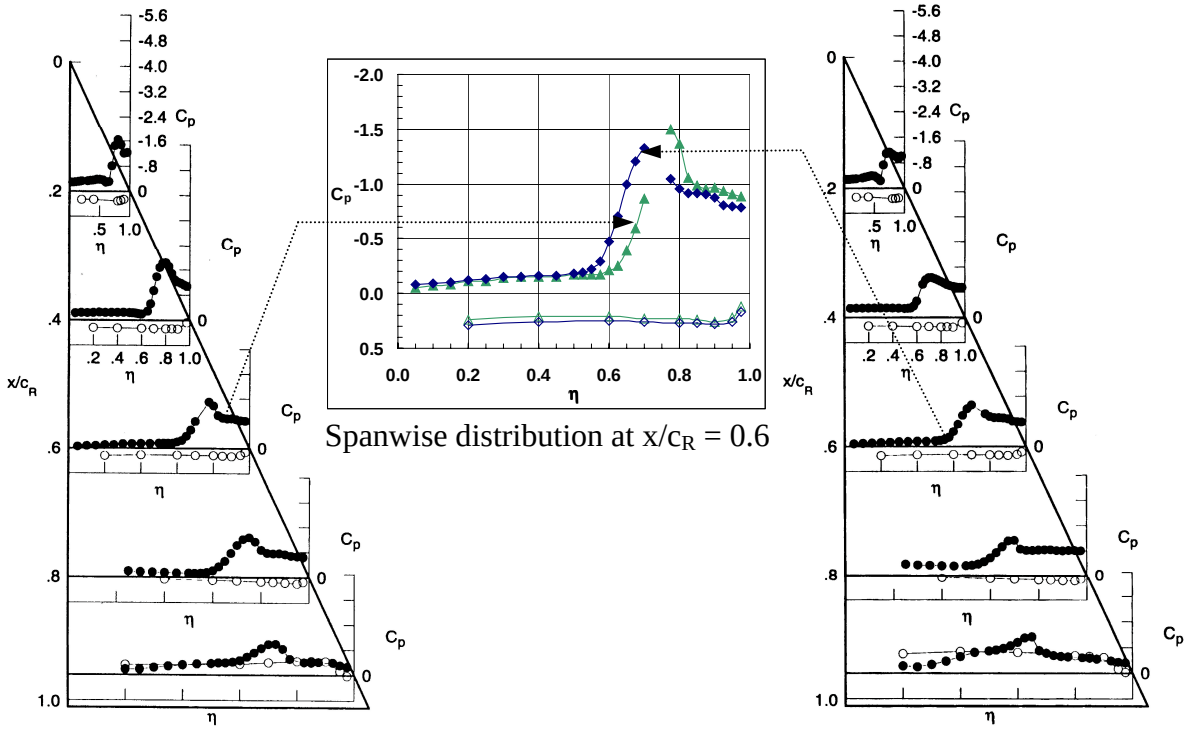

Fig. 10: Effect of Mach number on the pressure distribution of the A = 1.85 (Λ = 65°) sharp-edged delta wing at R = 6 • 10^6, α = 13° [15]

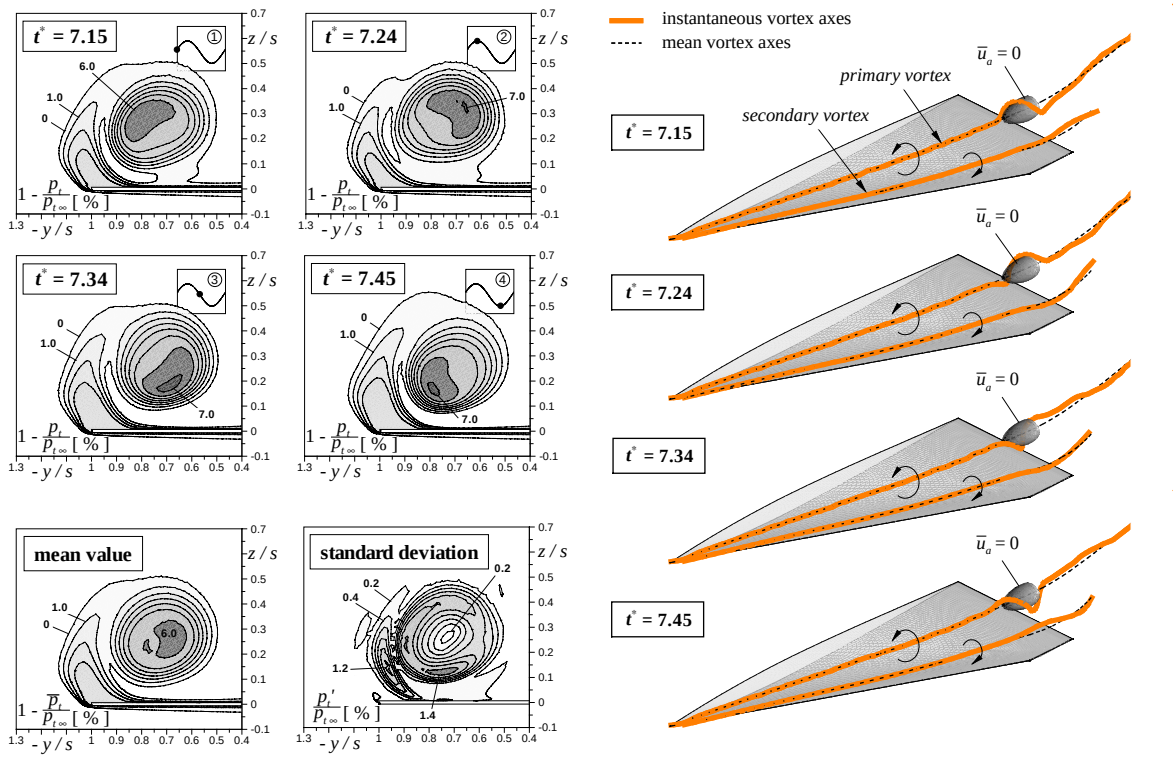

Fig. 11: Numerical simulation of vortex breakdown for the VFE-1 configuration at R = 1.55 • 10^6, M = 0.2, α = 21°, Navier-Stokes solutions with k – ω turbulence model: Total pressure losses at x/c_R = 0.95 and vortex axes for different time steps [24]

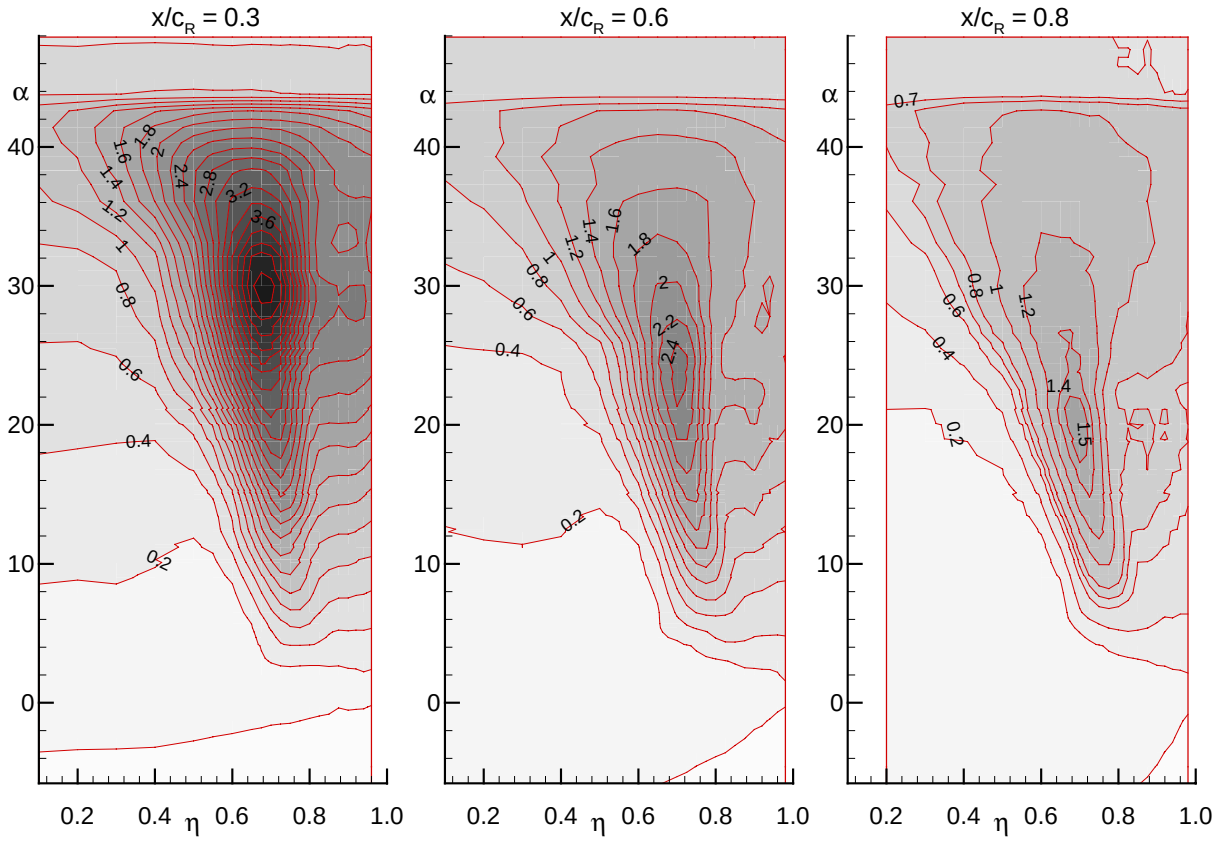

Fig. 12: Pressure distributions with lines c_p = const. in the sections at x/c_R = 0.3, 0.6 and 0.8 of the VFE-1 configuration for different angles of attack α, R = 3.1 • 10^6 [29]

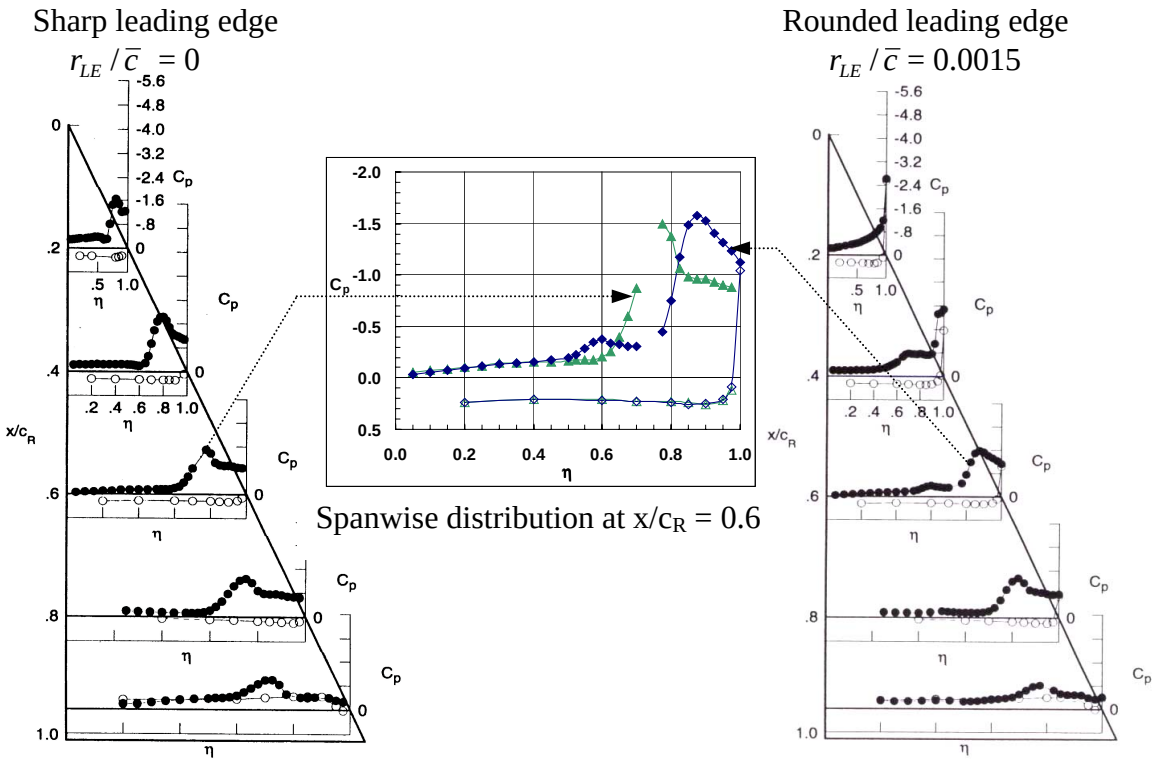

Fig. 13: Effect of leading edge bluntness on the pressure distribution of the A = 1.85 (Λ = 65°) delta wing at M = 0.4, R = 6 • 10^6, α = 13° [15]

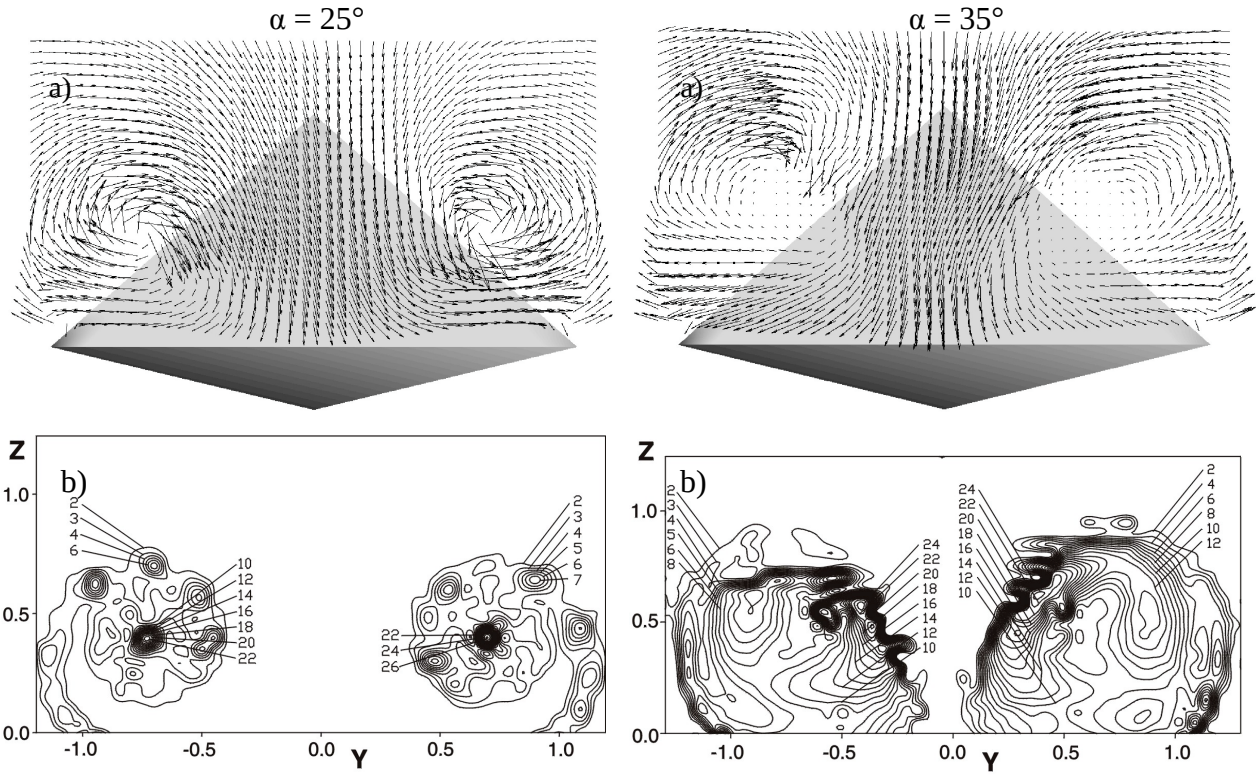

Fig. 14: Results of hot-wire measurements in the section at x/c = 0.9 of an A = 1 (Λ = 76°) delta wing at R = 1.7 • 10^6 according to [26]
a) Vectors of the mean crossflow velocity
b) Vertical rms velocity contours (in % of V)

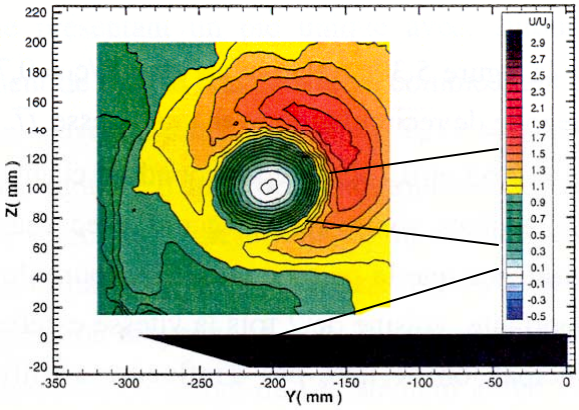

a) Lines $\overline{u}/V$ = const.

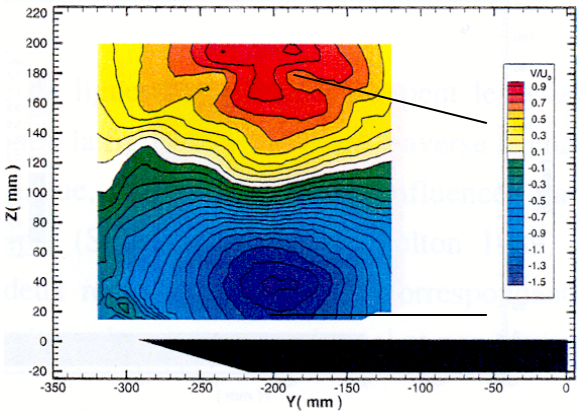

b) Lines $\overline{v}/V$ = const.

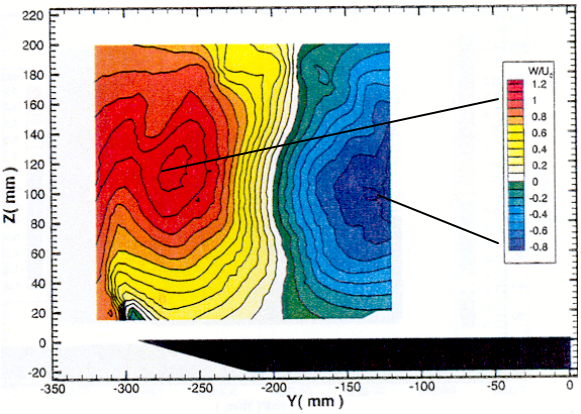

c) Lines $\overline{w}/V$ = const.

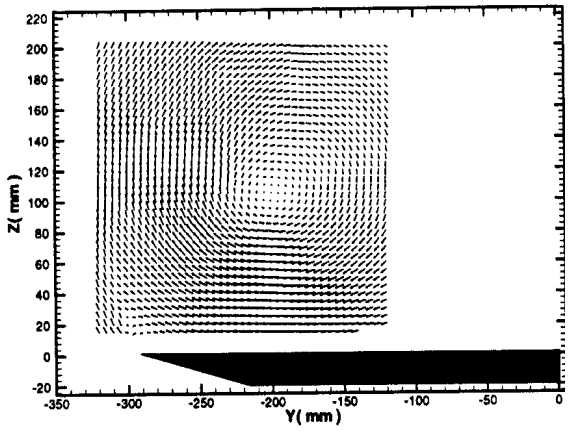

d) Mean crossflow velocity vectors

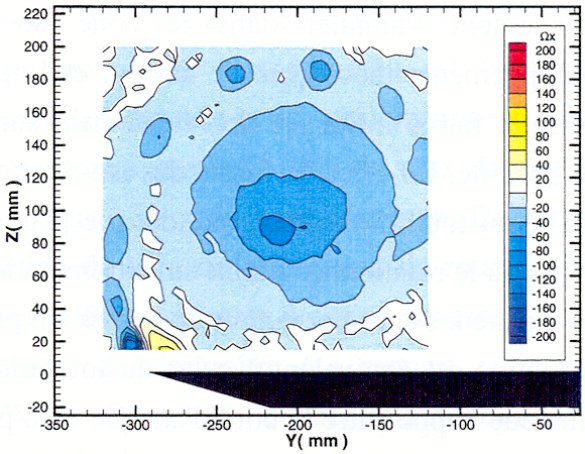

e) Axial vorticity Ω_x (c/V)

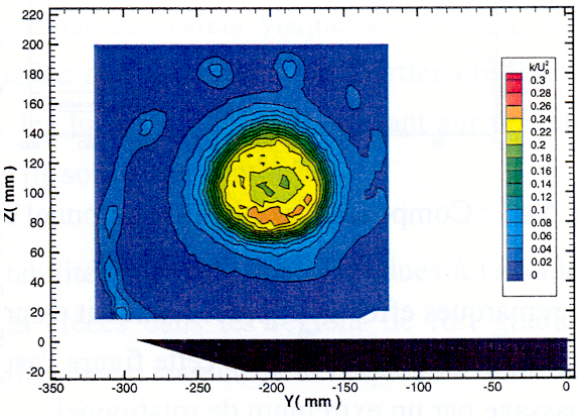

f) Turbulent kinetic energy k/V^2

Fig. 15: Results of LDV measurements in the crossflow plane at x/c = 0.84 of an A = 1.46 (Λ = 70°) delta wing at α = 27° [55]

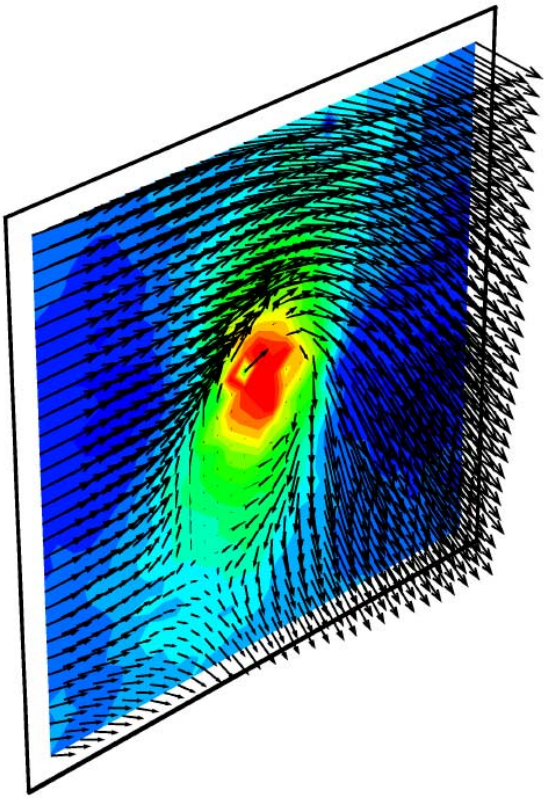

Fig. 16: Velocity distribution in the tip vortex of a helicopter blade measured by means of 3-component stereo PIV [64].

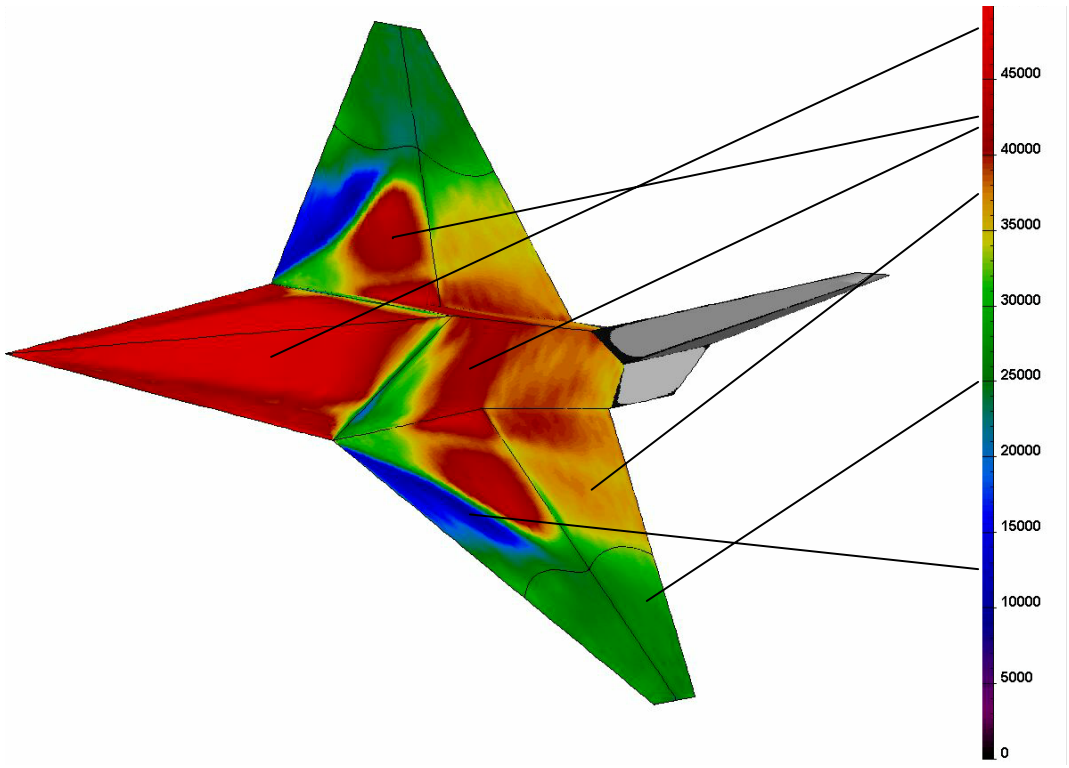

Fig. 17: Pressure distribution on the DLR-F7 configuration at M = 0.8, α = 10°. Result of PSP measurements. (Numbers in the legend indicate the absolute pressure in Pascal) [79].

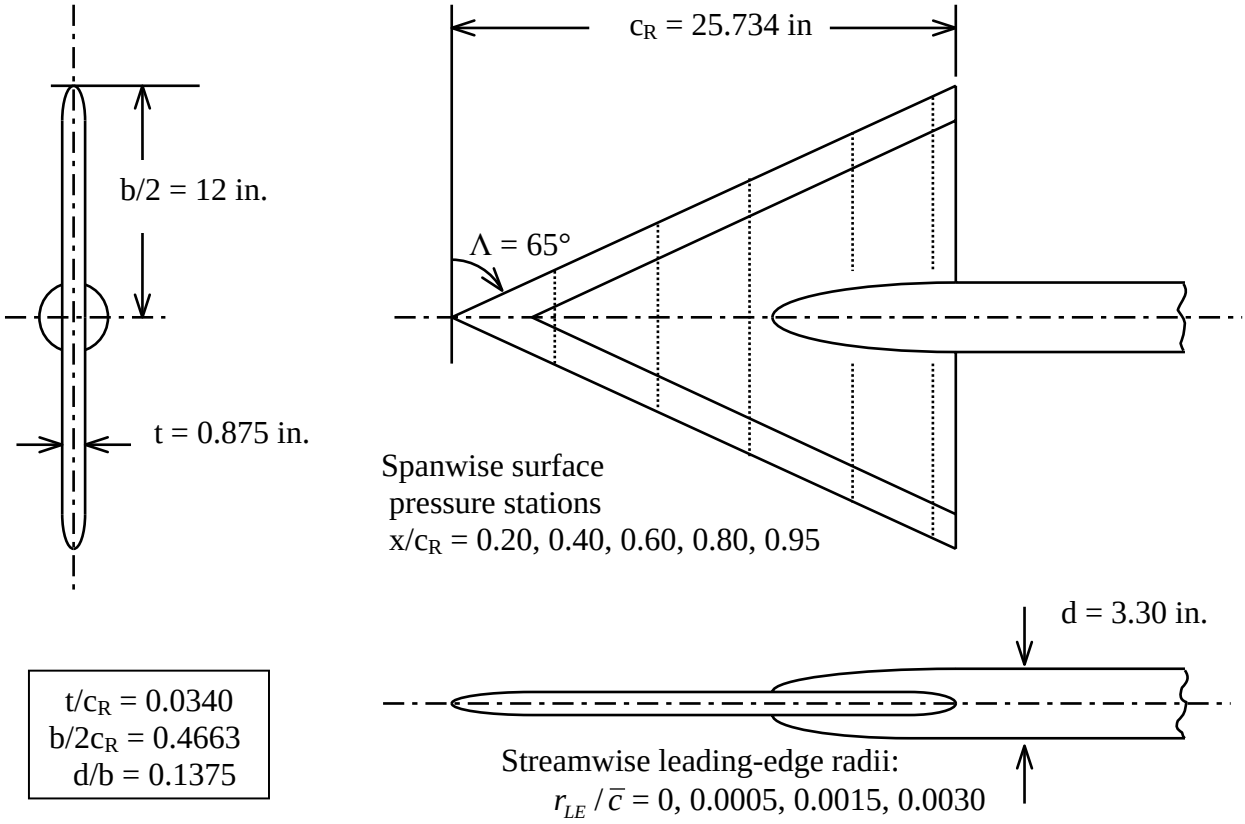

Fig. 18: NASA NTF delta wing configuration A = 1.85, Λ = 65°[15]

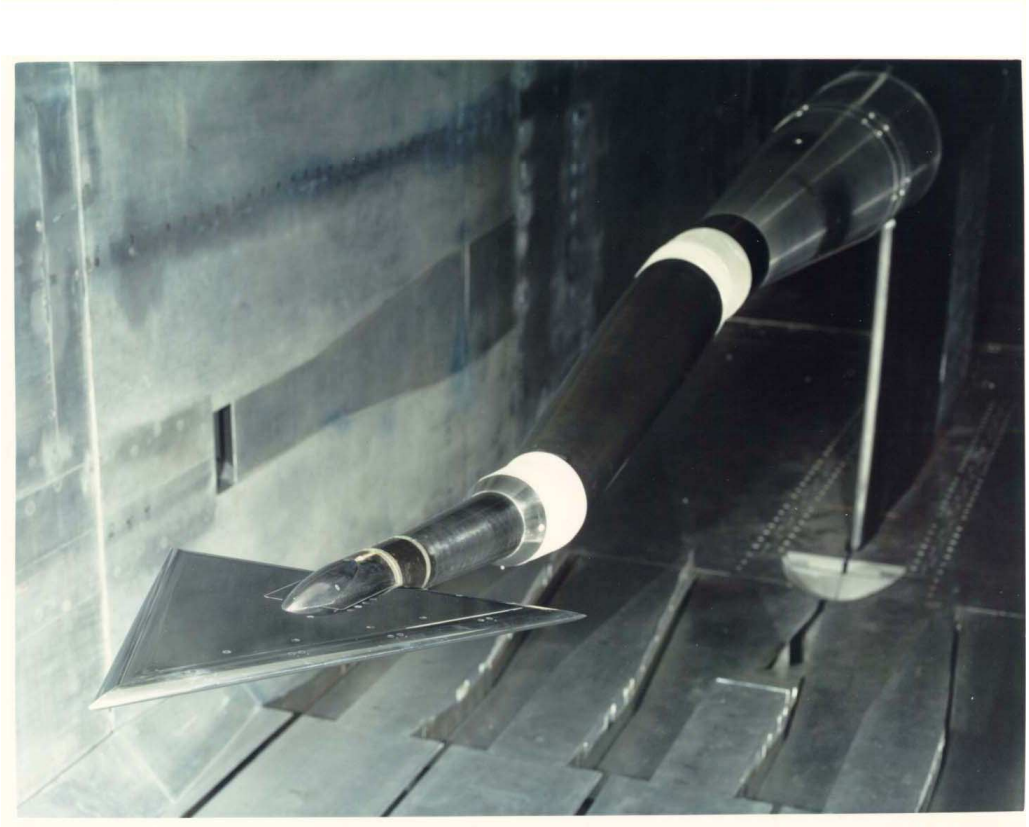

Fig. 19: A = 1.85 (Λ = 65°) delta wing at cryogenic tests in the National Transonic Facility (NTF), NASA Langley Research Center (by courtesy of J.M. Luckring)

This page has been deliberately left blank

Page intentionnellement blanche